Enhancing dielectric and piezoelectric properties of micro-ZnO/PDMS composite-based dielectrophoresis

Xiaoting Zhang, Minh-Quyen Le, Omar Zahhaf, Jean-Fabien Capsal, Pierre-Jean Cottinet, Lionel Petit

Version of Record: https://www.sciencedirect.com/science/article/pii/S0264127520303178
Manuscript_9bc38495d9d63f089b168f331d279f36

Enhancing dielectric and piezoelectric properties of micro-ZnO/PDMS composite-based dielectrophoresis

Xiaoting Zhang, Minh-Quyen Le*, Omar Zahhaf, Jean-Fabien Capsal, Pierre-Jean Cottinet, Lionel Petit.

Univ Lyon, INSA-Lyon, LGEF, EA682, F-69621, Villeurbanne, France
* Corresponding authors: minh-quyen.le@insa-lyon.fr

Abstract: This work aims to enhance the dielectric and piezoelectric properties of polydimethylsiloxane (PDMS) polymer filled with zinc oxide (ZnO) powders. Both ZnO nanoparticles and microparticles are used to prepare piezoelectric composites and a comparison of their dielectric responses is carried out. The experimental results reveal that a higher particle concentration gives rise to the increased dielectric permittivity of composites, especially when particles are aligned in the poling-direction-based dielectrophoretic process. Hence, the microparticles are chosen instead of the nano ones because the microscale facilitates the fabrication process of the composite, especially with high filler content. It also makes it possible to clearly record the movement of particles under alternating (AC) voltage application using optical microscopy. Significant improvement in the dielectric and piezoelectric behavior of the proposed composite has been successfully achieved via dielectrophoretic alignment of ZnO microparticles. This technique leads to increased connectivity between ZnO/ZnO interfaces, allowing for the creation of continuous aligned piezoelectric particles inside the polymer matrix. As a result, the piezoelectric effect is considerably boosted. Finally, the dielectric constant, as well as the charge coefficient of the ZnO particles, are estimated through theoretical approaches for composites containing particles arranged in chains or randomly dispersed. The model predictions are in good agreement with the experimental results. Furthermore, a finite element model (FEM) is developed using Comsol Multiphysics to evaluate these parameters in a 3D structure, which is then compared to those obtained by the above 2D-analytic models.

Keywords: nano/micro ZnO composites; structured materials, aligned particles, dielectrophoresis; piezoelectric properties, dielectric characterizations.

1. INTRODUCTION

Composites are materials that consist of at least two components that, when combined, produce a material with significantly different physical or chemical properties. Among them, embedding inorganic filler into polymer is a special method for preparing a new class of composite with enhanced functionality and a wide range of applications in diverse fields [1–4]. Over the last twenty years, increasingly prominent researchers have made efforts to explore and commercialize those multicomponent polymer systems [5–10]. This method combines the unique electric, magnetic, optical, thermal, and piezoelectric properties of inorganic particles at the nanoscale or microscale level with the advantages of the polymer matrix, such as excellent processability, flexibility, and stability [11–15]. Additionally, those composites afford ameliorated properties that are different from conventional materials and that can be tailored by varying the shape, size, and concentration of fillers and determined by the underlying parameters, like filler dispersion, intercalation, and filler-matrix interaction. Such development in smart advanced material surely propelled the growth of additive-manufacturing-based 3D/4D printing technology [16–20].

It is well known that zinc oxide (ZnO) is one of the most significant II-VI semiconductor materials attracting alternative interest and research, especially in the application of optoelectronic, electromechanical, electrochemical, photovoltaic devices, etc., owing to its excellent intrinsic properties [21–26]. ZnO nanoparticles have attracted increasing attention due to the quantum effect and large polymer-filler interaction area. Encapsulation of the ZnO powders in a polymer matrix can integrate the

piezoelectric property and mechanical property with superior flexibility. Various synthesis techniques and electrical characteristics of ZnO powder/polymer composite thin film have been studied [27–29]. Moreover, ZnO is a biocompatible material, which opens the door to specifically targeting medical and health applications such as *ex vivo* and *in vivo* flexible sensors by taking advantage of the piezoelectric property. Recently, a ZnO-poly(sodium 4-styrenesulfonate)/poly(vinyl alcohol) (PVA) thin film was reported for dynamic strain sensing and behavior comparable to those of commercial poly(vinylidene fluoride) (PVDF) thin film [30]. It is well known that piezo-ceramic lead zirconate titanate (PZT) is brittle and expensive and has a high loss factor and that piezoelectric polymers possess a considerably low piezoelectric constant [31,32]. Therefore, it is promising to fabricate large-scale ZnO/polymer composite thin film with improved mechanical, electric, and piezoelectric properties.

Newnham *et al.* [33] demonstrated that in a multiphase composite system, electromechanical coupling and piezoelectric properties can be controlled by arrangement of the constituent phase, allowing for an increase in the number of connectivity patterns. It was also mentioned that the charge coefficient (d_{33}) of the piezoelectric composites was strongly dependent on the pattern of connectivity, which elaborated on the interspatial relationships between two phases. In a study reported by Yamada *et al.* [34], the ceramic phase was randomly dispersed within a polymer matrix, generally referred to as 0-3 composites, and exhibited only promising piezoelectric properties at high filler content, i.e., around 67% volume fraction. At low concentration, a large discrepancy in the dielectric properties of two phases, including resistivity and permittivity, causes the unbalanced electric field distribution. In other words, electric charge is exerted more on the polymer than on the particles, resulting in low piezoelectric properties [35,36]. On the other hand, the 1-3 connectivity composites, defined as continuous fibers aligned in one dimension, normally have higher piezoelectric coefficients despite having a more complicated fabrication and higher cost compared to the 0-3 composites [37,38]. Dielectrophoretic activity can therefore be widely employed to create an intermediate state between a 0-3 and 1-3 connectivity pattern by manipulating particles [39–41], nanotubes [42,43], and nanofibers [36,44] in composite through application of an AC electric field.

It has been demonstrated that an improvement in the piezoelectric, dielectric, and pyroelectric properties of composite with PZT in the epoxy matrix was obtained by dielectrophoretic alignment of ferroelectric particles [36,45,46]. Based on this approach, submicron barium titanate (BaTiO3) powders dispersed in an uncured silicone elastomer could be re-organized into anisotropic composite [47]. Belijar *et al.* proposed a new technique for monitoring particle alignment of Epoxy/BaTiO3 composites, based on the online measurement of the dielectric permittivity. As a result, the permittivity variations can be correlated to the particle chains and to their growth [48]. Besides applications relating to structuration of particles formation and locations, these novel materials open up new application fields for piezoelectric sensing and energy harvesting. For instance, in automobile tires where low frequency and high strains are present, a small quantity of energy can be converted from the environment to electricity, allowing to power electronics such as wireless sensors [49]. In addition, dielectrophoretically processed polymers were also applied within microfluidic systems, which are well suited for applications such as separation and sorting [50,51], trapping and assembling [52,53], patterning [54,55], purification [56], and characterization [57,58] in a wide range of environmental, biological, and clinical applications [59]. Additionally, dielectrophoresis can also be employed in the fabrication of nano and microelectronic devices, for instance sensors (gas, chemical, force, and biosensors) [60–62], field-effect transistors [63,64], oscillators [65], and several other electronic and optical devices [66,67]. There are many other future applications that can be explored using dielectrophoresis-based techniques such as tissue engineering, controlled culture, and advanced manipulations of particles in lab-on-a-chip systems [68].

To the best of our knowledge, most of the studies dedicated to dielectrophoretically structured piezoelectric composite treated principally with the well-known ceramic ferroelectric particles (e.g. BaTiO3, PZT, etc.), while none of them has yet explored the ZnO particles. Recently, Md. Abdulla Al Masud and Zoubeida Ounaies investigated the dielectric properties of aligned ZnO/PDMS composites but its impact on the piezoelectric response has not been reported [69]. Kumar *et al.* focused on nano-gap electrode assembly by the dielectrophoresis of ZnO nanoparticles, but not on piezoelectric composite [70].

In this work, the dielectric and piezoelectric properties of structured micro-ZnO composites with volume fractions from 14% to 44% are investigated and compared to composites of randomly dispersed ZnO particles. The experimental results are evaluated with the predictions of theoretical approaches for relative permittivity (ε_r) and the charge coefficient (d_{33}) as a function of the ZnO volume fraction of the composites. Then, the correlation is discussed. To better highlight the influence of particle size, some of experimental tests are also conducted on nano-ZnO composites. Because of the high surface energy that originated from the ZnO nanoparticles, it is difficult to achieve nanocomposite with high volume fraction. Over 21% of volume, the ZnO nanoparticles easily agglomerate and precipitate out of solution, resulting in very high viscosity of dispersion that are unsuitable for composite film fabrication. Consequently, the nano-ZnO composites are elaborated with lower concentration than the micro-ZnO composites, which significantly limit enhancement of the nanomaterials in dielectric and piezoelectric responses. Moreover, the use of microparticles enables the facilitation of not only the fabrication process but also dielectrophoretic observation under a low-cost optical microscope which can be clearly visible at the microscale but not the nanoscale. Based on these reasons, only micro-ZnO composite is chosen to be performed in dielectrophoretic study.

The structure of the paper is organized as follows. Firstly, Section 2 describes the steps used in the casting method for preparing nano- and micro-ZnO/PDMS films. Secondly, Section 3 describes the dielectrophoretic alignment of ZnO particles in an uncured PDMS solution through a varying high-voltage application whose amplitude and frequency are chosen based on a digital microscope observation. Fabrication of the 1-3 structured composites is therefore carried out under the best dielectrophoretic configuration defined by the above processing parameters. Then, electric field distribution within particles and its surroundings is performed thanks to Comsol FEM. Thirdly, Section 4 illustrates the characterization method for dielectric spectroscopy and piezoelectric response. After that, the results and discussion are detailed in Section 5. Analytical models, together with a FEM based Comsol simulation were correlated to the measured data, making a possibility to assess the permittivity constant and the charge coefficient of the ZnO particles. Finally, the conclusion and future works are discussed in Section 6.

2. MATERIALS AND PROCESS

2.1. Material selection

ZnO nanopowder (80~100 nm diameter, 99.9% purity) and micropowder (~10 µm diameter, 99.9% purity) were purchased from US Research Nanomaterials Inc. with a mass density of 5.6 g/cm^3. A Sylgard-184 silicone elastomer kit including a base and curing agent was acquired from Trademark of the Dow Chemical Company. The polydimethylsiloxane (PDMS) elastomer was heated after the mixing of two components at a mass ratio of 10 (silicone elastomer base): 1 (silicone elastomer curing), allowing for the obtaining of a polymer with mass density ρ = 1.1 g/cm^3. The raw materials used in the composite fabrication process were treated without any chemical modification.

For nano-ZnO/PDMS composites, low volume content is chosen including 8%, 13%, 17%, and 21%. Nonetheless, for micro-ZnO/PDMS composites, higher concentration of 14%, 24%, 34%, and 44% is performed. This difference is due to the fact that particle's size has significant effects on the dielectric relaxation time and the chain mobility of the polymer molecules. If compatibility between the particles and the matrix is relatively good, the macromolecules in the vicinity of the particles have restricted mobility and this will increase the viscosity of the composite. This is the case of nanocomposite where a larger number of polymer molecules come in contact with the particles thanks to high specific surface area between them. Consequently, smaller size of particles will be lead to the higher viscosity of dispersions. For that reason, nanoparticles are commonly used to make composites with low concentration, i.e. inversely to microparticles.

2.2. *Elaboration based casting method*

To fabricate different volume fractions of composites, ZnO micro/nanoparticles and PDMS polymer contents were calculated based on the volume mixing law given by:

$$\phi_z = \frac{M_z}{M_z + M_p} = \frac{\rho_z * \varphi_z}{\rho_z * \varphi_z + \rho_p * \varphi_p} \quad (1)$$

$$\varphi_z + \varphi_p = 1 \quad (2)$$

where φ and ϕ are, respectively, the volume fraction and mass fraction; and M and ρ denote the mass and mass density, respectively. The subscripts z and p correspond to the ZnO particles and polymer matrix, respectively.

Figure 1 displays the material elaboration based on the classical casting method. Firstly, the nanoparticles or microparticles were mixed with the PDMS solution (Figure 1a) at a given ratio according to the volume fraction of ZnO defined in Eq. (1). Secondly, 30-minute ultrasonication (Hielscher Ultrasound Technology, UP400S) was carried out for the whole solution (Figure 1b) under a ventilate table (I Type Cabinet B - ADS air Depoussiéré), allowing for the perfect uniform dispersion of ZnO powder in the PDMS polymer. Thirdly, a curing agent was added to the solution, which was then constantly stirred for 10 minutes until a homogenous substance was obtained (Figure 1c). After that, the beaker of liquid composite was put in a vacuum drying oven (Memmert, VO 400) at 20℃ for 30 minutes to completely evacuate the air bubbles trapped during the early mixing process (Figure 1d). Subsequently, the uncured ZnO/PDMS mixture was poured into a specific mold to be cast as a film on a glass substrate (Figure 2Figure 1e). The thickness of the film could be controlled by a specific blade; normally, a 0.5mm thickness was required in this experiment. Finally, the casting film was put into the oven at a temperature of 100℃ for 35 minutes to speed the heat curing reaction (Figure 1f). Through this fabrication method, nano-ZnO/PDMS (Figure 2a) composite and micro-ZnO/PDMS (Figure 2b) composite with a different volume fraction of ZnO particles were successfully obtained.

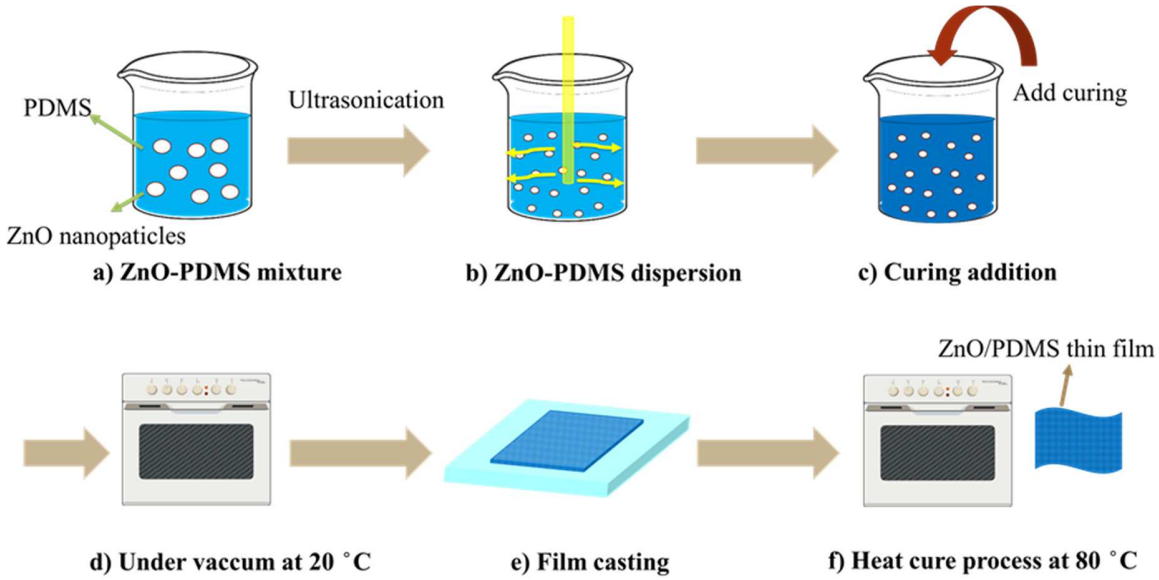

Figure 1. The schematic displays the fabrication of ZnO/PDMS nanocomposite or microcomposite. First steps involves in (a) mixing of ZnO nano or microparticles with PDMS polymer at a specific ratio, and (b) dispersing ZnO particles through ultrasonication to obtain homogeneous suspensions. Step (c) is to add curing agent to the uncured mixture, and (e) degas solution under vacuum at 20°C to remove air bubbles. (f) Finally, the composite is cast as a thin film, then (g) cured at 100°C for 35 minutes.

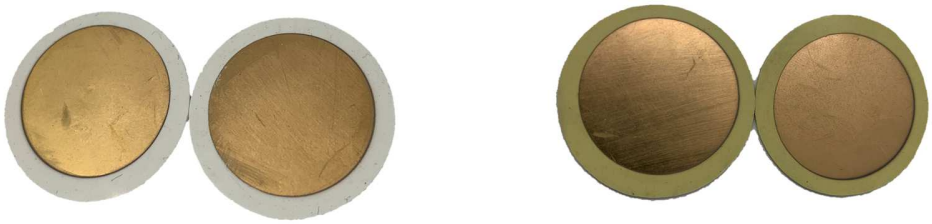

(a) (b)

Figure 2. Elaborated samples based flexible PDMS polymer filled with ZnO particles (a) Nano-ZnO/PDMS sample, and (b) Micro-ZnO/PDMS sample.

3. BUILDING A STRUCTURED ZNO COMPOSITE BY DIELECTROPHORESIS

The dielectrophoretic effect can be utilized to manipulate particles dispersed in a fluid medium and offers a simple alternative approach to create oriented particle-filled polymer composites with anisotropic properties. When an electric field is applied to an uncured thermosetting polymer, the dispersed particles form chains, which are fixed in place when the matrix is cured [36]. To enhance the piezoelectric effect of PDMS polymer filled with nano/micro ZnO particles, structured material via dielectrophoresis has been investigated. In dielectrophoresis, a force is exerted on a particle when it is subjected to a non-uniform electric field induced by the alternating current polarization of two metallic electrodes. The strength of the force depends strongly on the medium and the electrical properties, shape, and size of the particles. The frequency and amplitude of the electric field matter as well [71]. This section aims to provide a preliminary study based on a microscopic imaging technique that enables the determination of the most appropriate parameters of the excited input electric field, together with a description focusing on dielectrophoretic manipulation.

3.1. Preliminary analysis

Considering a dielectric sphere particle that suspends homogeneously in a fluid matrix under a non-uniform electric field, an electric dipole moment is formed with the positive and negative charges center displaced on the opposite sides of the particle. Accordingly, the dielectrophoretic force exerted on a dielectric particle can be deduced as [72]:

$$F_{\mathrm{dep}} = 2\pi\varepsilon_0\varepsilon_{\mathrm{m}}R^3\,\mathrm{Re}[\mathrm{CM}(\omega)]|\nabla E_{\mathrm{rms}}^2| \tag{3}$$

where R is the radius of the particle; ε_{m} is the relative permittivity of the polymer matrix; ∇E_{rms} is the gradient of the root-mean-square of the applied electric field; Re[CM(ω)] denotes the real part of CM(ω); and CM(ω) denotes the frequency-dependent Clausius-Mossotti factor that can be explained as [68]:

$$CM(\omega) = \frac{\varepsilon_p^* - \varepsilon_m^*}{\varepsilon_p^* + 2\varepsilon_m^*} \tag{4}$$

The real part of CM(ω) is, thus, given by:

$$Re[CM(\omega)] = \frac{\omega^2(\varepsilon_p - \varepsilon_m)(\varepsilon_p + 2\varepsilon_m) + (\sigma_p - \sigma_m)(\sigma_p + 2\sigma_m)}{\omega^2(\varepsilon_p + 2\varepsilon_m)^2 + (\sigma_p + 2\sigma_m)^2} \tag{5}$$

where ε^*, σ, and ω are the complex permittivity, the conductivity, and the angular frequency, respectively. The subscripts p and m represent the property of the particle and the surrounding medium, respectively. According to Eqs. (3)–(5), the magnitude of the dielectrophoretic force is greatly impacted by the dielectric properties of the particles and matrix, as well as the amplitude and frequency of the electric field. Therefore, the optimal external electric field in terms of amplitude and frequency should be carefully

considered in the dielectrophoretic experiment to effectively exploit the piezoelectric effect of the ZnO nano/microparticles.

The dielectrophoretic orientation process can be observed under a digital microscope (AVEN, Mighty Scope). To clearly record the movement of particles, a low concentration mixture (i.e., 3% vol. of micro-ZnO) after vacuum processing in the uncured state was filled up between two parallel copper electrodes (see Figure 3) through which high-voltage excitation was driven. The degree of particle alignment was monitored and compared between samples at different amplitudes and frequencies of the external voltage application. As we discussed in Eq. (3), the dielectrophoretic force is proportional to the amplitude of the applied electric field, while the speed movement of particles is determined by the balance between the dielectrophoretic force and other factors like drag force. Figure 4b indicates that under low-voltage excitation corresponding to 0.5 V/µm, the ZnO particles still randomly separate, which is similar to the phenomenon obtained without the electric field as depicted in Figure 4a. This result highlights the fact that the dielectrophoretic force exerted on particles under 0.5 V/µm is not sufficient to complete their orientation in 60 seconds. On the other hand, at a higher input electric field of 1 V/µm, the composite clearly shows an obvious orientation trend along the filed direction, i.e., a vertical direction from top to bottom as illustrated in Figure 4c. When the electric field increases to 2 V/µm (Figure 4d), an aggregation phenomenon near copper electrodes occurs, leading to a considerable increase in the probability of short-circuiting, which perhaps results from air bubbles and/or a limited electrical breakdown of the PDMS polymer. As a result, the electric field of 1 V/µm was considered to be the most adequate for the fabrication of aligned ZnO/PDMS composite.

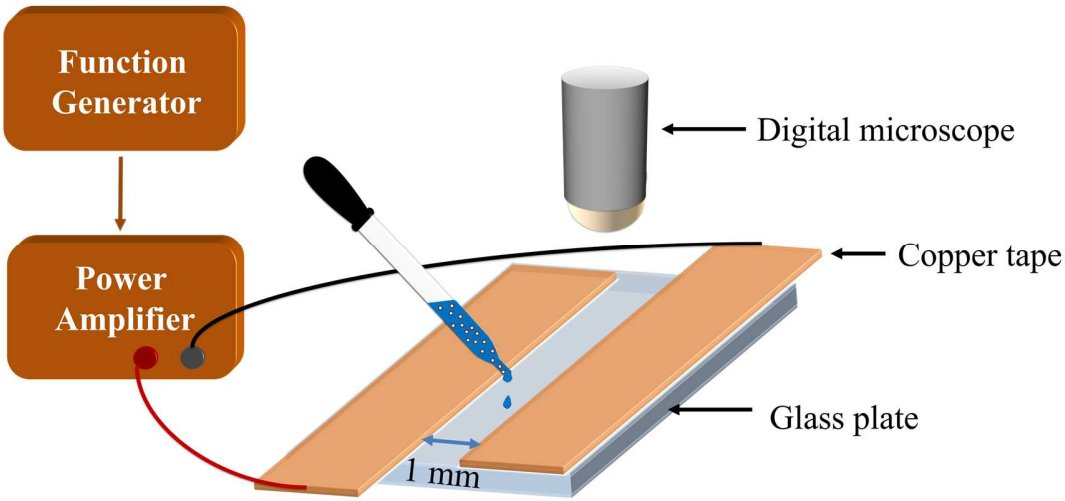

Figure 3. Experimental setup for structuring PDMS solution filled with 3% vol. of ZnO particles performed under microscopic observation.

Another relevant parameter that should be taken into account for the dielectrophoretic experiment is the frequency of the input voltage. A practical test is carried out using the 3% vol. ZnO/PDMS composites under the same electric field of 1 V/µm amplitude but with four different frequencies, including 0.2 Hz, 2 Hz, 20 Hz, and 200 Hz. As can be seen in Figure 5, all samples achieve the same alignment position and are in a stable state after 60 seconds from the beginning, confirming that the frequency has less of an impact on the degree of orientation as opposed to the amplitude of the electric field during the dielectrophoresis process. In the next subsection, an AC electric field of 1 V/µm amplitude and 2 Hz frequency will be selected to be exerted on a well-dispersed ZnO/PDMS mixture during the heat curing process to form stable and structured material. For better observation of the particle alignment, an optical microscope (Olympus) was utilized to check the composite structure after 3 minutes under the above-defined electric field. Images with a magnification of 40X (Figure 6a), and 100X (Figure 6b) were recorded and clearly show the formation of aligned particle chains along the field direction.

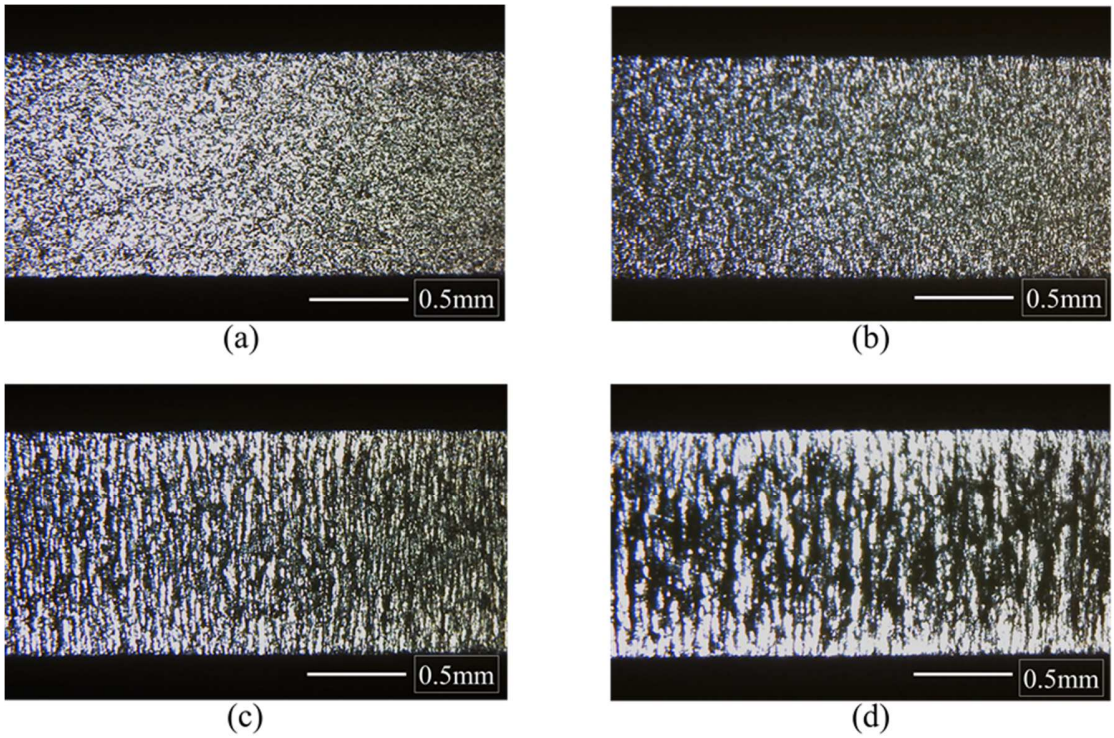

Figure 4. Microscopic observation of non-cured ZnO/PDMS mixture with 3% volume fraction: (a) before applying the electric field. At 60s after applying the electric field with frequency 2Hz and amplitude at (b) 0.5V/µm, (c) 1 V/µm, and (d) 2 V/µm.

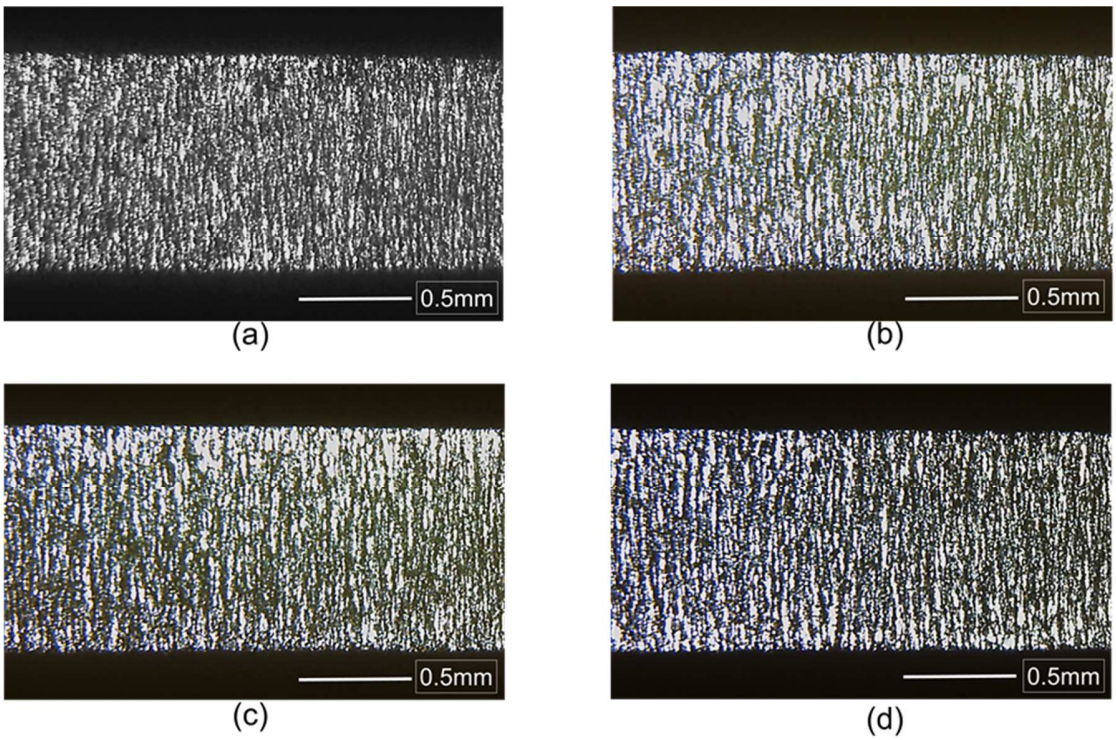

Figure 5. Microscopic observation of non-cured ZnO/PDMS mixture with 3% volume fraction at 60s after applying an electric field of 1 V/µm with a frequency of (a) 0.2 Hz, (b) 2Hz, (c) 20 Hz, and (d) 200 Hz.

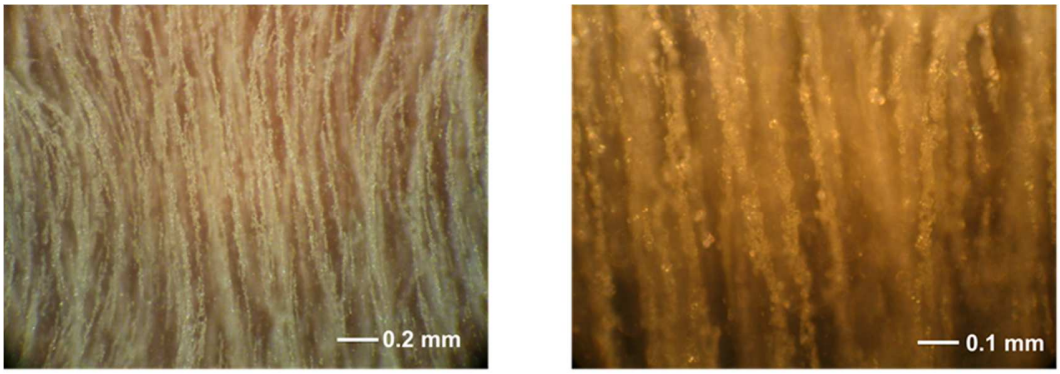

Figure 6. Image-based optical microscope of non-cured micro ZnO/PDMS mixture with 3% volume fraction after 3 minutes from applying an electric field of 1V/µm amplitude and 2 Hz frequency with a magnification of (a) 40X and (b) 100X.

3.2. Dielectrophoretic manipulation

The process of preparing the structured ZnO/PDMS composite was similar to the process of fabricating the random dispersed composite as previously described in Subsection 2.2, except for the last two steps, (f) and (g), of Figure 1. As illustrated in Figure 7, a layer consisting of a 0.5-mm-thick styrene plate (Evergreen Scale Models, Inc.) with a circular 25 mm diameter hole that was carefully filled with the uncured ZnO/PDM solution. The sample holder was then clamped between two parallel copper electrodes on which high voltage was applied. A thick, heavy circular brass plate of 500g was put on the top electrode to provide enough pressure for obtaining flat and compact samples. Afterward, the whole sample and support were placed into an oven (Votsch IndustrietechnikTM, VT7004) at a constant temperature of 80°C for 1 hour. The electrodes were externally connected to a functional voltage generator (Agilent, 33210A) whose signal was amplified 1000 times via an amplifier (Trek, Model 20/20C). Lastly, both random and aligned thin films were cut into circular samples of a 25 mm diameter by using a cylinder steel mold with a circular cavity of the same diameter. Thin gold electrodes of 20 mm-diameter and 25µm-thick were then deposited on two sides using a sputter coater (Cressington, 208HR) under the condition of 0.4 mA and 60 seconds.

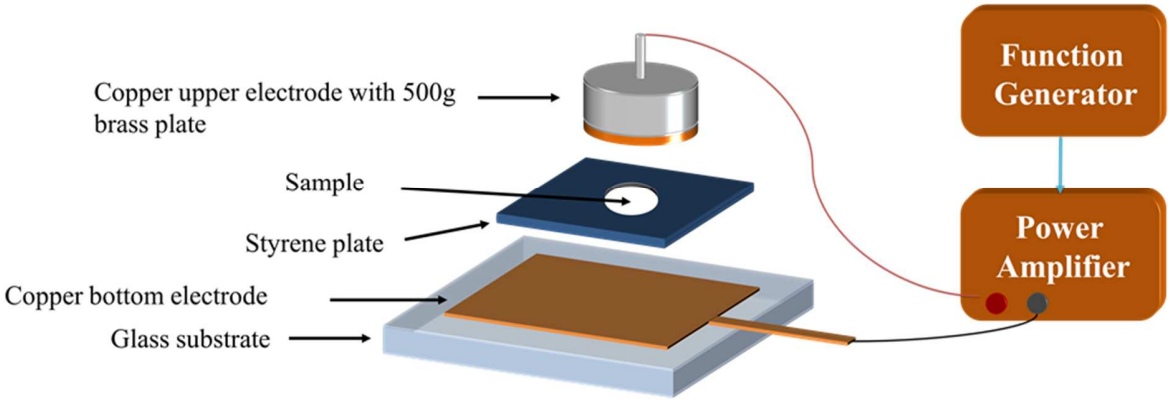

Figure 7. Schematic drawing of the mold used for the dielectrophoresis process under a high-amplitude electric field.

3.3. Electric field distribution based 2D Comsol model

In order to have an idea about the distribution of the field within the particles and its surroundings, 2D Comsol model is carried out. In the FEM simulation, we define ZnO circular particle with a diameter of 10 µm, embedded in PDMS polymer with 80 µm long × 70 µm wide. The bottom of the matrix is electrical ground whereas a potential of 70 V is applied on the top, allowing to drive an electric field of 1V/µm to the whole matrix. The density of free charges in the materials is considered to be zero as the dielectric loss in ZnO composite under such an electric filed is negligible. Figure 8 illustrated the electric field distribution in random and structured microcomposites with a different ZnO volume fraction of 14% and 44%. For all samples, the electric filed level is greatly higher in the polymer matrix than in the particles, especially around the particles, the electric filed becomes maximum. This result is consistent to the one reported on Pedroli *et al*. [73], where the electric field is always more significant in the material with lower dielectric permittivity (in polymer, for instance). In the structured materials (Figure 8 b and d), as the axes of the particle chains are oriented perpendicular to the active surface (i.e. applied by an electric potential), the electric field would mainly affect the interparticle interactions within the same chain. This leads to homogenous electric field distribution of all particles, which is contrary to the case of the random matrix (Figure 8 a and c).

In addition, the results of Figure 8 allow to confirm that the ZnO particle is a dielectric isolation, as the electric filed driven within the particles is significantly lower than the threshold value above which, ZnO passes from isolator to conductor. Several studies was investigated to characterize the electrical properties of ZnO material. In [74], current-voltage characteristics of a photo-conducting organic liquid-crystal film based Zinc octakis(b-decoxyethyl)porphyrin (i.e. ZnODEP) was performed, allowing to deduce the electric field threshold of around 0.15 – 0.2 V/µm. Alternatively, Ahmad *et al.* demonstrated that under low applied electric filed, the relative permittivity of the ZnO powder was constant, and then drastically drop when the electric field attains the threshold value (i.e., approximately 0.15 – 0.9 V/µm). Actually, changes of applied field level will cause a sudden increase in the conduction regime, leading to a significant fall in capacitance, which affects the relative permittivity of the material. Based on these above results in literatures, it is obvious that in our case, the electric filed applied on the particles (less than 0.1V/µm) is not sufficient enough to make them conductive. In the subsection 5.2, dielectric characteristics will be carried out, again, allowing to confirm isolating properties of the ZnO composites.

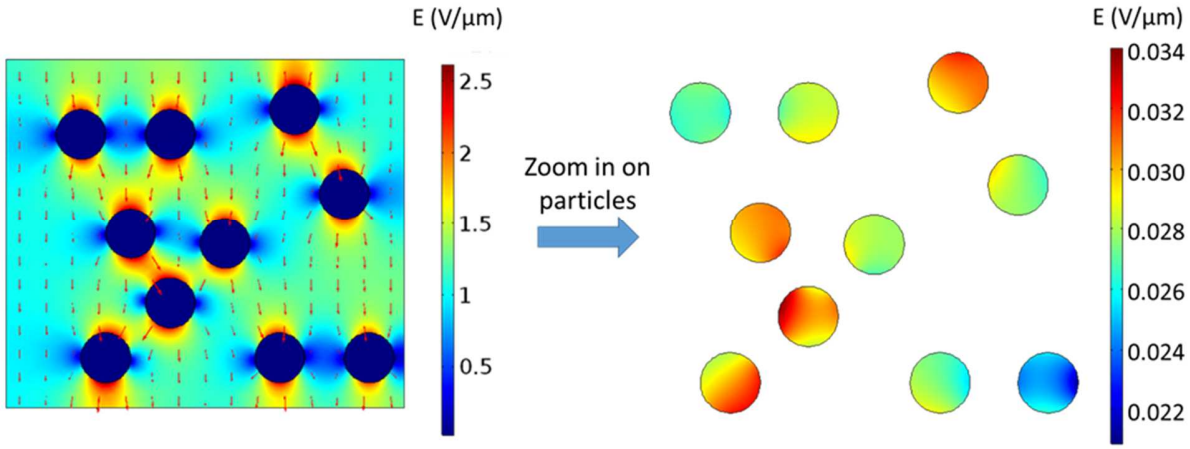

a) Random ZnO/PDMS composite with 14% volume fraction

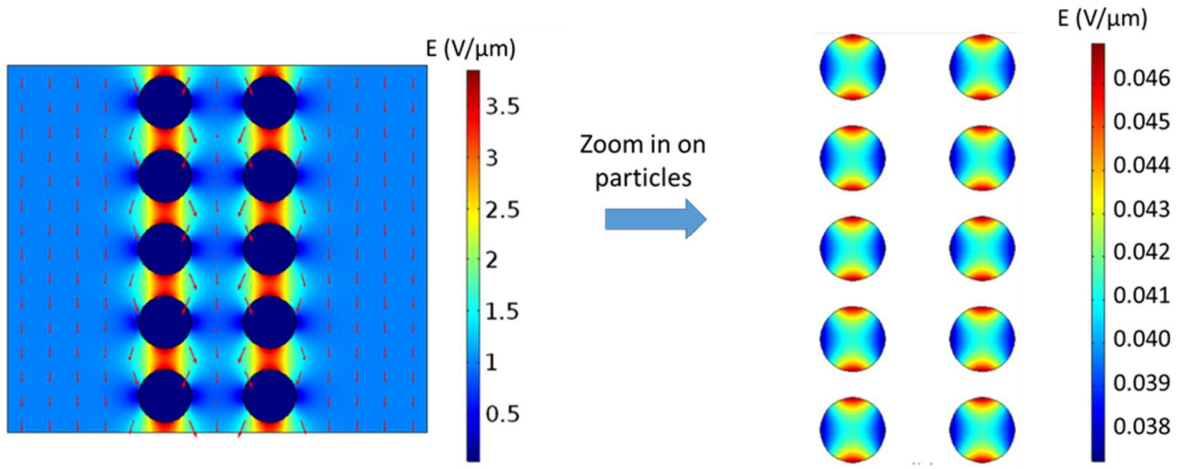

b) Structured ZnO/PDMS composite with 14% volume fraction

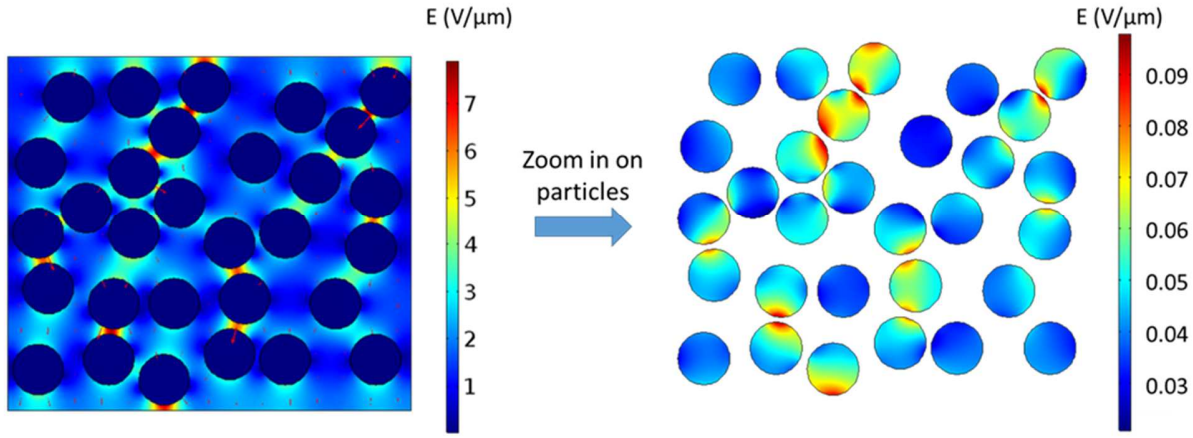

c) Random ZnO/PDMS composite with 44% volume fraction

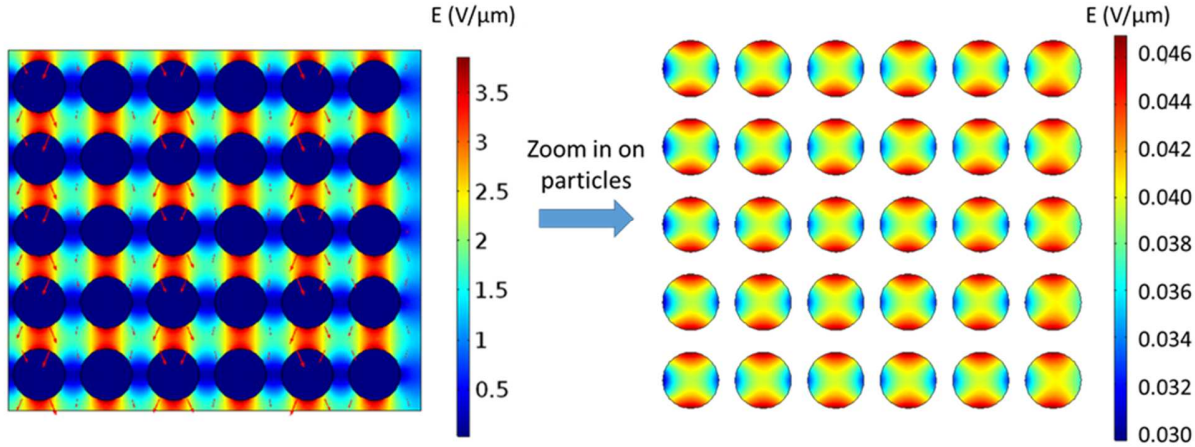

d) Structured ZnO/PDMS composite with 44% volume fraction

Figure 8. Electric field distribution in random and structured microcomposites with a different ZnO volume fraction (on the left-hand side), and a closer view of the particles (on the right-hand side).

4. CHARACTERIZATION METHODS

4.1. Dielectric characterization

Broadband dielectric spectroscopy of the ZnO/PDMS composite was obtained by Solartron 1296 Dielectric Interface combined with a 1255 HF Frequency Response Analyzer. The accurate estimation of the dielectric spectra was measured under an external alternating voltage of 1V amplitude and a wide frequency range from 0.1Hz up to 1MHz in an ambient environment.

4.2. Piezoelectric characterization

The piezoelectric charge coefficient of the fabricated composite was measured using a specially designed setup with high sensitivity, as shown in Figure 9. The sample was clamped between upper and lower electrodes. Dynamic mechanical excitation was driven by a piezoelectric stack actuator (PI 246-50) with tunable amplitude and frequency controlled by a waveform generator (Agilent, 33500B) together with a voltage amplifier (Trek, Model 20/20C). In this experimental test, a mechanical frequency equal to 1 Hz was chosen, whereas the voltage amplitude varied to obtain different levels of force exerted on the sample. The charge coefficient d_{33} can be estimated as:

$$d_{33} = \frac{D}{T} = \frac{\frac{Q}{S_{ative}}}{\frac{F}{S}} \tag{6}$$

where S_{active} and S denote the surface of the gold electrode and the sample, respectively; Q denotes the electric charge; D is the electric displacement (or charge density); and T and F, respectively, denote the mecanical stress and applied force. To avoid measurements of parasitic deformations, the clamping electrodes should have the same diameter as the gold electrode (i.e., around 20 mm).

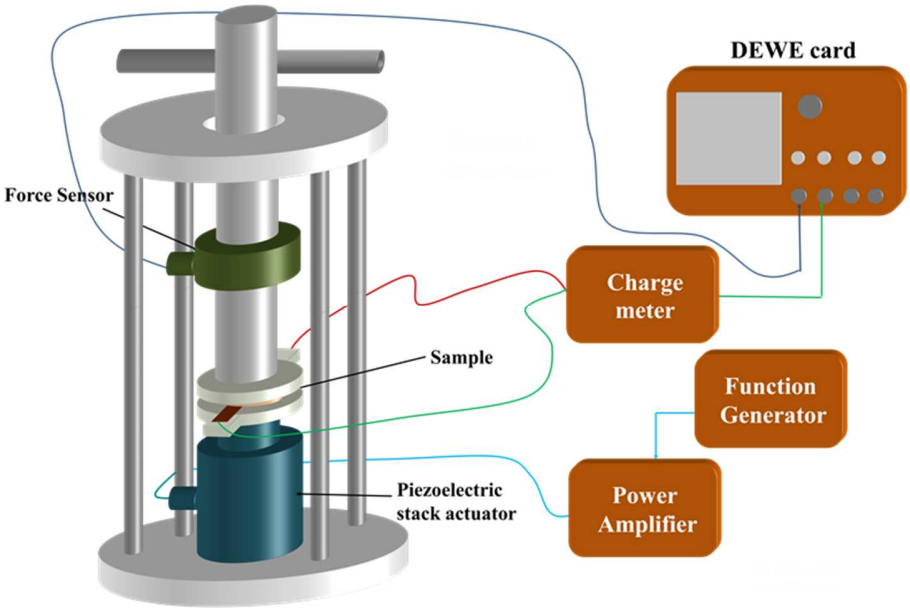

Figure 9. Experimental setup dedicated to electromechanical characterization.

During the movement, the force F was quantified via a load sensor (HBM) and the electrical charge Q was measured through a high-sensitivity charge meter (KISTLER, Type 5015). The charge density D and the mechanical stress T can therefore be easily deduced, allowing for obtaining the value of the piezoelectric coefficientd_{33}. Finally, real-time signals were simultaneously recorded using DEWE software (Sirius 8XSGT). Post-data treatment was performed with the Origin software.

5. RESULTS AND DISCUSSION

5.1. Dielectric property of random nano- and micro-ZnO/PDMS composites

Figure 10a displays the variation of the dielectric constant versus frequency for the PDMS polymer incorporated with a different volume fraction of ZnO nanoparticles. It can be seen that the dielectric constant of the pure PDMS and the composites with low concentrations (e.g., 8% or 13%) is somewhat stable for a large range of frequency. On the other hand, when the ZnO volume content is increased to 17% or 23%, the dielectric constant significantly increases under low dynamic excitations (i.e., 0.1Hz-1Hz) and decreases with higher frequency. This phenomenon can be ascribed to the interfacial polarization, also known as the Maxwell-Wagner-Sillars effect. The increase in the interfacial area in polymer nanocomposites sets interfacial polarization as a predominant physical effect for their dielectric performance [76,77]. Without external electric field, if the particles are homogeneously dispersed in the polymer matrix, no dipole moment related to the ZnO/PDMS interface contributes to the bulk dielectric constant. Usually, high particle concentrations lead to a transition from the ZnO/polymer interface to the ZnO/ZnO interface, where the electron can be trapped at electronic states. As a result, the generation of interfacial dipole moments can occur, giving rise to significant variation in the dielectric permittivity under low frequencies [78]. Conversely, with higher dynamic excitation, i.e., above 1 kHz, the permittivity can be considered to be frequency-independent; even a slight decreasing trend has been observed due to the relaxation mechanism of the ZnO-PDMS composite. To some extent, the dielectric relaxation times is closely related to the conductivity. For instance, the relaxation time is usually small in metals and can be large in semiconductors and insulators. Since high ZnO content gives raise to enhanced conductivity of the composites, it conducts to somehow faster response and as a result, reducing relaxation time. Subsequently, the decreasing trend in dielectric constant is particularity more visible at materials with higher content of ZnO.

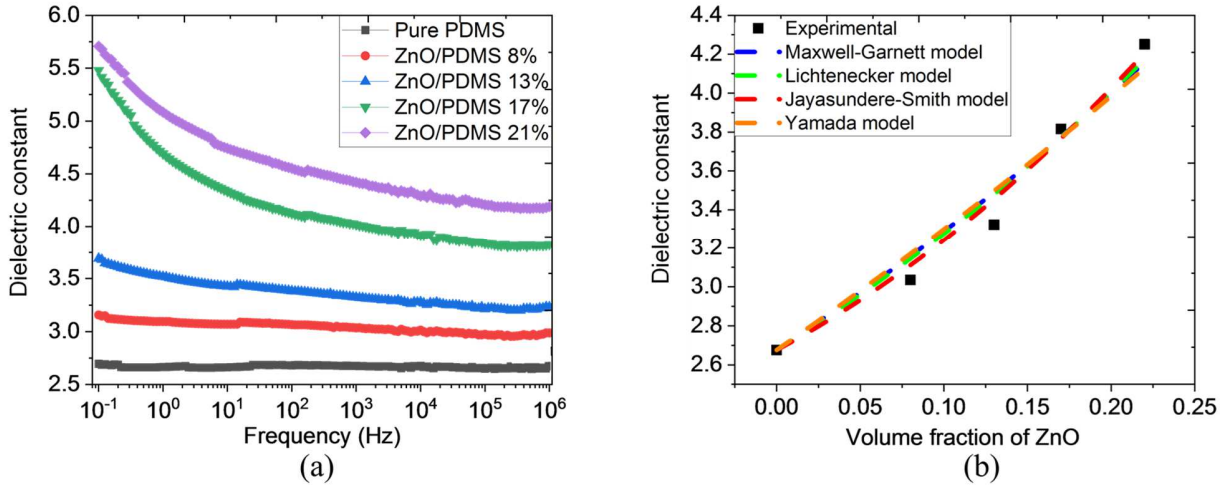

Figure 10. Variation of the dielectric constant of nano-ZnO/PDMS composites as a function of (a) frequency and (b) ZnO concentration measured at 1 kHz together with a comparison of associated models.

As observed in Figure 10b, the experimental dielectric constant of nano-ZnO/PDMS composite substantially increases with the ZnO content at 1 kHz. Various theoretical models developed by Maxwell-Garnett, Lichtenecker, and Jayasundere-Smith are used to predict the dielectric constants plotted in Figure 10b. For the sake of simplicity, these approaches are supposed to be frequency-independent. As a result, a deeper analysis of the dielectric property is performed under a dynamic of 1 kHz, above which frequency-variation of the permittivity is relatively moderate.

The Maxwell-Garnett model is suitable for a two-phase composite with spherical particles in a continuous medium given by [79]:

$$\varepsilon_{eff} = \varepsilon_m \frac{2\varepsilon_m+\varepsilon_p+2f_p(\varepsilon_p-\varepsilon_m)}{2\varepsilon_m+\varepsilon_p-f_p(\varepsilon_p-\varepsilon_m)} \quad (7)$$

where f_p is the volume content of ZnO in composite; and ε_m, ε_p, and ε_{eff} represent the dielectric constant of the polymer matrix, particles, and composites, respectively. The relative permittivity of PDMS (ε_m) is known as 2.68, according to technical Data sheet of "SYLGARD™184 Silicone Elastomer". This result is also confirmed by dielectric spectroscopy using SOLARTRON (Figure 10a) where the dielectric constant of the pure PDMS sample is almost frequency dependent.

Lichtenecker logarithmic law is described for a two-component system based on the logarithmic dielectric constants of each component [80]:

$$\log \varepsilon_{eff} = f_p \log(\varepsilon_p) + f_m log \varepsilon_m \quad (8)$$

where f_m is the volume fraction of the polymer matrix in the composite. Jayasundere and Smith developed an equation to calculate the effective dielectric constant, including interactions between neighboring spheres [81]:

$$\varepsilon_{eff} = \frac{f_m\varepsilon_m+\varepsilon_p f_p\left[\frac{3\varepsilon_p}{\varepsilon_p+2\varepsilon_m}\right][1+\frac{3f_p(\varepsilon_p-\varepsilon_m)}{\varepsilon_p+2\varepsilon_m}]}{f_m+f_p\left[\frac{3\varepsilon_p}{\varepsilon_p+2\varepsilon_m}\right][1+\frac{3f_p(\varepsilon_p-\varepsilon_m)}{\varepsilon_p+2\varepsilon_m}]} \quad (9)$$

Yamada *et al.* studied a binary system composed of the continuous medium and ellipsoidal particles and proposed a dielectric model that can be expressed as [34]:

$$\varepsilon_{eff} = \varepsilon_m[1 + \frac{nf_p(\varepsilon_p-\varepsilon_m)}{n\varepsilon_m+f_m(\varepsilon_p-\varepsilon_m)}] \quad (10)$$

where *n* is a shape-dependent parameter, relating to the morphology of ellipsoidal particles. It is noticed that such a parameter is considered only for the Yamada model, as opposed to the other models, in which the shape of particles has not been considered for the estimation of the dielectric constant.

The fitting between experimental data and theoretical models allows for the obtaining of the relative permittivity ε_p of the PDMS polymer filled with ZnO nanoparticles as summarized in Table 1. Interestingly, different analytical models give slight variations of the dielectric constant, e.g., from 13.4 to 22. However, as highlighted in Figure 10b, all models lead to an excellent trend with respect to experimental data, reflecting high reliability of the theoretical approach for PDMS composite with the volume content of ZnO particles up to 20%. Compared to the other models, that of Jayasundere-Smith results in the highest coefficient of determination (i.e., *R-squared* or R^2 equals 0.985). Furthermore, this approach allows for the taking into account of the interactions between the neighboring particles as opposed to the Maxwell-Garnett and Lichtenecker estimations. Thus, the expected dielectric constant of the nano-ZnO composite is chosen equal to approximately 13.4. This value is used in the Yamada equation (Eq. 10) to determine the shape factor *n* (cf. Table 1).

Table 1. Fitting parameters from various models of nano-ZnO/PDMS composite

Model	ε_m	ε_p	n	R^2
Maxwell-Garnett model	2.68	22.06 ± 2.92	-	0.969
Lichtenecker model	2.68	20.12 ± 1.56	-	0.974
Jayasundere-Smith model	2.68	13.40 ± 0.65	-	0.985
Yamada model	2.68	13.40	4.97± 0.71	0.962

Figure 11a illustrates the dielectric spectroscopy of the micro-ZnO/PDMS composites with a different volume fraction from 0% to 44%. As expected, the relative permittivity $\boldsymbol{\varepsilon_p}$ is greatly enhanced as a function of particle concentration, where the 44% vol. sample leads to a dielectric content of 19 under a low frequency of 0.1 Hz, which is a six times increase as opposed to the pure one. A multiple factor of five times has been achieved at a higher dynamic of 1 kHz. As discussed before, interfacial dipole moments at the ZnO/ZnO interface contribute to the frequency-dependent behavior of the dielectric constant for the samples with high particle concentration. In the case of micro-ZnO/PDMS composite, this effect is prominent when the concentration is above 34% volume (cf. Figure 11a).

Figure 11b plots the measured and theoretical dielectric constants of PDMS polymer filled with different volume content of ZnO microparticles. Analytical parameters found by fitting the experimental data and theoretical models of Eqs. (7) – (10) are summarized in Table 2. It can be noticed that the Lichtenecker and Jayasundere-Smith models yield a similar prediction of ε_p around 125 with a coefficient of determination R^2 very close to 1, reflecting an excellent correlation between empirical data and estimated values. Substituting the relative permittivity $\varepsilon_p = 125$ in the Yamada model produces the shape-dependent parameter of $n = 6.62 \pm 0.55$, which is higher than the one obtained in the case of nano ZnO particles (cf. Table 1). Unlike the other models, the Maxwell-Garnett approach fails to match the experimental data of the micro-ZnO/PDMS composite, especially at a volume fraction over 20%. This result is consistent with the one reported on previous publications. [82,83].

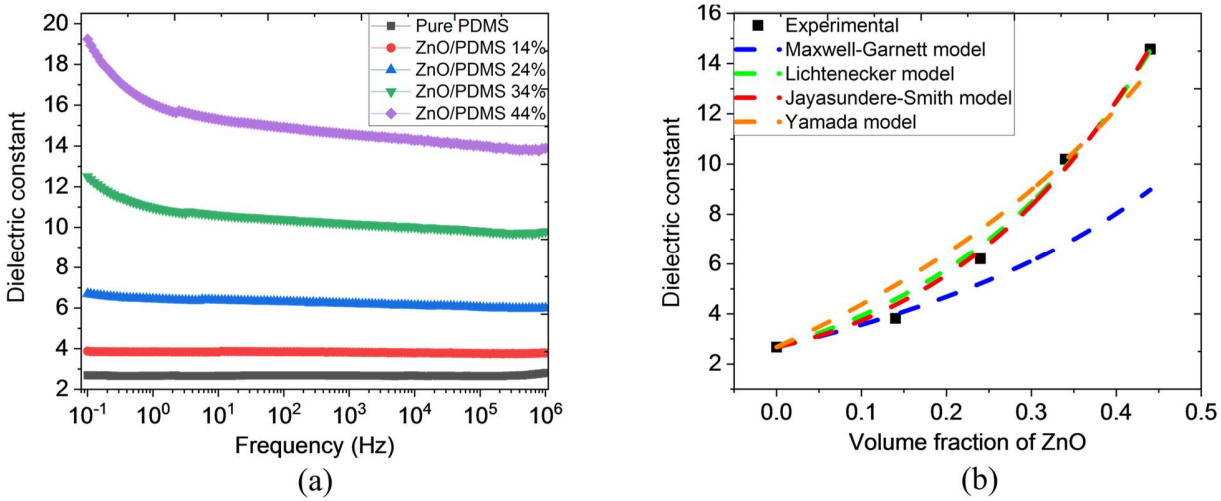

Figure 11. Variation of the dielectric constant of the random micro-ZnO/PDMS composite as a function of (a) frequency and (b) ZnO concentration measured at 1kHz together with a comparison of associated models.

Table 2. Fitting data from various models of the micro-ZnO/PDMS composite

Model	$\boldsymbol{\varepsilon_m}$	$\boldsymbol{\varepsilon_p}$	$\boldsymbol{n}$	$\boldsymbol{R^2}$
Maxwell-Garnett	2.68	-	-	0.543
Lichtenecker	2.68	125.07 ± 8.19	-	0.990
Jayasundere-Smith	2.68	125.48 ± 18.22	-	0.994
Yamada	2.68	125	6.62± 0.55	0.960

All above results allow to confirm further advantage of micro-ZnO composites with respect to the nano-ones. Concretely, micro-ZnO composites allow to:

- higher dielectric permittivity. For instance, the dielectric permittivity (at 1kHz) of the micro-sample and nano-sample respectively equals to 4.5 and 7, for a volume fraction of around 21%–24%. It is due to the fact that the permittivity of the micro-particles (ε_p ~ 125) is higher to the one of the nanoparticles (ε_p ~ 20), which is based on the analytic models;
- higher maximum volume fraction (44% compared to 21% as in the case of the nanocomposite, leading to better dielectric and piezoelectric responses);
- easier fabrication process. Indeed, nanoparticles lead to very high viscosity of composite, making difficult dispersion even with ultrasonication. As a result, they are usually used for fabrication of composite with low concentration (maximum 21% in our case). Moreover, most of process based on nano-materials needs special care and treatment for manipulators, as a result, more complex equipment are necessary with respect to the case of micro-materials;
- simpler observation of particle chains during dielectrophoretic process under a low-cost digital mciroscope, which is impossible for the nanocomposite, considering the limited magenification.

The following studies will focus on the effect of dielectrophoretic structuring on dielectric behavior as well as the piezoelectric property of the micro-ZnO composites.

5.2. Effect of dielectrophoretic structuring on dielectric and piezoelectric properties

This subsection aims to demonstrate that the dielectrophoretic effect with oriented particles in the early stages of cure has a significant impact on the dielectric and piezoelectric properties of micro-ZnO/PDMS composites.

Besides the analytical models of Bowen [39] and Van den Ende [36] used for structured composites, an alternative approach to predicting the effective dielectric constant, as well as the charge coefficient of such materials, is based on FEM using Comsol Multiphysics with a 3-D simulation. The composites consist of a cube-shaped PDMS polymer embedded with ZnO spherical particles with a 5µm radius. As shown in Figure 12a–d, different volume fractions of 14%, 24%, 34%, and 44% were respectively designed by keeping the same amount of ZnO, but with a different volume of polymer matrix. In this model, particles are aligned with and perfectly connected to each other to form a chain-like structure. The bottom part of the matrix was fixed and grounded. Figure 12e–h represents the level of the resulting charge density under a compression stress of 1 MPa in the vertical direction, reflecting the image of the piezoelectric response.

Figure 13a depicts the dielectric constant of aligned micro-ZnO/PDMS composites at a large frequency range of 0.1 Hz to 1MHz. Samples were elaborated with different concentrations of piezoelectric ZnO particles, which are similar to the study reported in subsection 5.1. The results of Figure 11a and Figure 13a demonstrate that the aligned 1-3 composites lead to significantly improved dielectric permittivity with respect to the 0-3 composite. Actually, at a low frequency of 0.1 Hz, a two-fold increase has been achieved for the sample elaborated with a 44% vol. fraction of ZnO powder, whereas there was a 3.5-fold increase for the 14% sample. In the event of a higher dynamic, e.g., at 1 kHz, enhancement in dielectric property between the aligned and random mixtures is less significant, corresponding to 1.5-fold and two-fold improvement for the 44% and 14% composites, respectively. Consequently, regardless of the frequency range, dielectrophoresis results in better permittivity enhancement for lower-concentration composites compared to those with a higher filler content.

To better assess the influence of the dielectric response versus the ZnO volume fraction, Figure 13b illustrates the experimental data of oriented and random materials at 1 kHz, above which their relative permittivity is supposed to be frequency-independent. To determine the physical parameters related to the ZnO/PDMS composite, two approaches have been investigated, consisting of a Comsol modeling/simulation as well as the analytic theory developed by Bowen *et al.* [39].

The Bowen model is applied on 2-D structured composites with aligned particles along the poling direction. The equation of the dielectric constant is given by:

$$\varepsilon_{eff} = f_p[\frac{r\varepsilon_p\varepsilon_m}{\varepsilon_p + r\varepsilon_m} + f_m\varepsilon_m)] \quad (11)$$

where r is the ratio of the average particle size to the effective inter-particle distance; ε_m denotes the relative permittivity of PDMS; and ε_p denotes the relative permittivity of ZnO microparticles (i.e., ~ 125, as previously determined in subsection 5.1). Based on the best correlation between the experimental data to the Bowen model, R is estimated as being approximately 24.3.

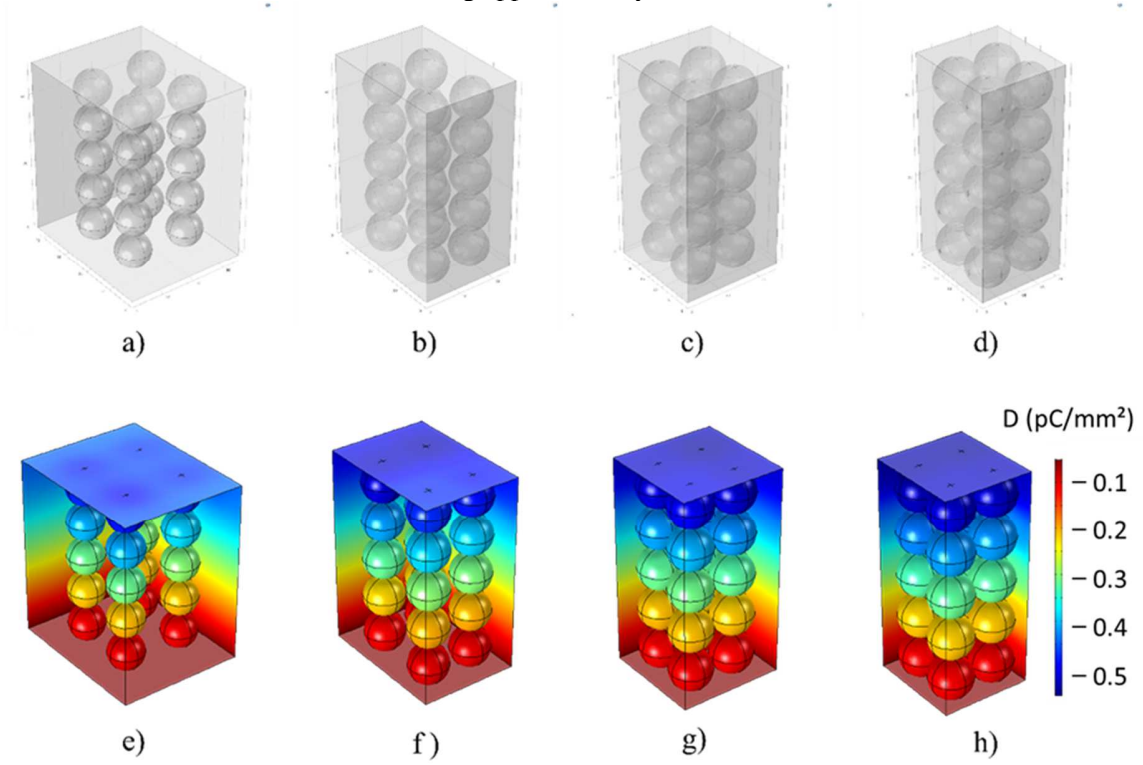

Figure 12. A 3D model of the structured ZnO/PDMS composite with a volume fraction of (a) 14%, (b) 24%, (c) 34%, and (d) 44% using Comsol Multiphysics. Images (e) to (f) are the corresponding charge density under an applied compression stress of 1MPa in the vertical direction.

In Comsol Multiphysics, the effective permittivity (ε_{eff}) of the composite can be calculated according to the following formula [84]:

$$D = \varepsilon_0\varepsilon_{eff}E \quad (12)$$

where D and E are, respectively, the charge density and the electric field and ε_0 is the vacuum permittivity. The input parameters, as well as the fitted result, are summarized in Table 3. As shown in Figure 13b, both the Comsol and Bowen models lead to a linear relationship between the dielectric constant and the ZnO fraction. Nonetheless, the FEM simulation leads to a much superior dielectric constant (ε_p) of ZnO microparticles (~ 218) than the Bowen calculation (~ 125). Tests carried out on Comsol demonstrate that increasing the distance between ZnO particles can decrease the effective permittivity of the composite. However, the inter-particle distance depends on the particle size as well as the parameter R determined from the Bowen model, which cannot be freely modified. Based on an estimation of the determination coefficient R^2, it is obvious that the adjustment quality of the Bowen model is more adequate than that of Comsol simulation. Finally, the main difference between these two approaches stems principally from the fact that 3D architecture was taken into account in the FEM, whereas a simple 2D design was used in the Bowen model.

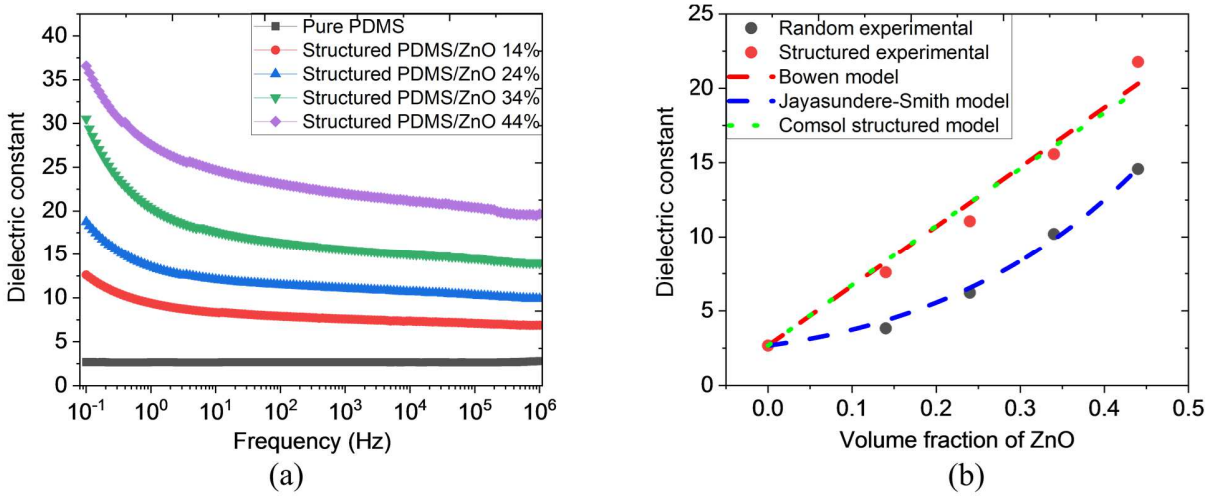

Figure 13. (a) Variation of the dielectric constant as a function of frequency for structured PDMS composites filled with different content of ZnO microparticles. (b) Experimental and theoretical dielectric constant versus ZnO concentration under an AC applied voltage of 1kHz and 1V amplitude.

Table 3. Fitting data in the structured micro-ZnO/PDMS composite

Model	ε_m	ε_p	r	R^2
Bowen	2.68	125	24.3 ± 1.5	0.978
Comsol	2.68	218	-	0.831

In order to see whether or not losses in dielectric material (the so-called tanδ) remain small over the considered frequency range (i.e. 1Hz–1MHz), Figure 14 illustrates frequency-dependent tanδ of the 1-3 and 0-3 microcomposites with different percentage of ZnO piezoelectric particles. As expected, the loss tangent in dielectric polymer increases with the piezoelectric concentration as higher ZnO content leads to increase conductivity of the composite. It can be seen that the pure PDMS exhibits very low and constant losses, which are mainly due to the dielectric losses, and not to the conduction losses. Similar behavior is observed for all ZnO composites at high frequencies (i.e., from 100 Hz), confirming that losses can be negligible in the Comsol simulation as well as in the analytical model (i.e. studied at 1 kHz). At low frequencies (1–10 Hz), on the other hand, tanδ is more considerable because of dominant conduction effect. Obviously, the 1-3 piezocomposite causes higher losses compared to the 0-3 random structure, since the aligned particle chains facilitate the conduction mechanism, giving raise to increase leakage current in the dielectric material. Although the structured composites with high ZnO content leads to increase conduction losses at low frequencies; all samples performed in this study behave as good dielectric materials with stable permittivity and insignificant losses. These results are consistent to those of subsection 3.3, again, allowing to confirm the isolating properties of ZnO particles under low applied electric field.

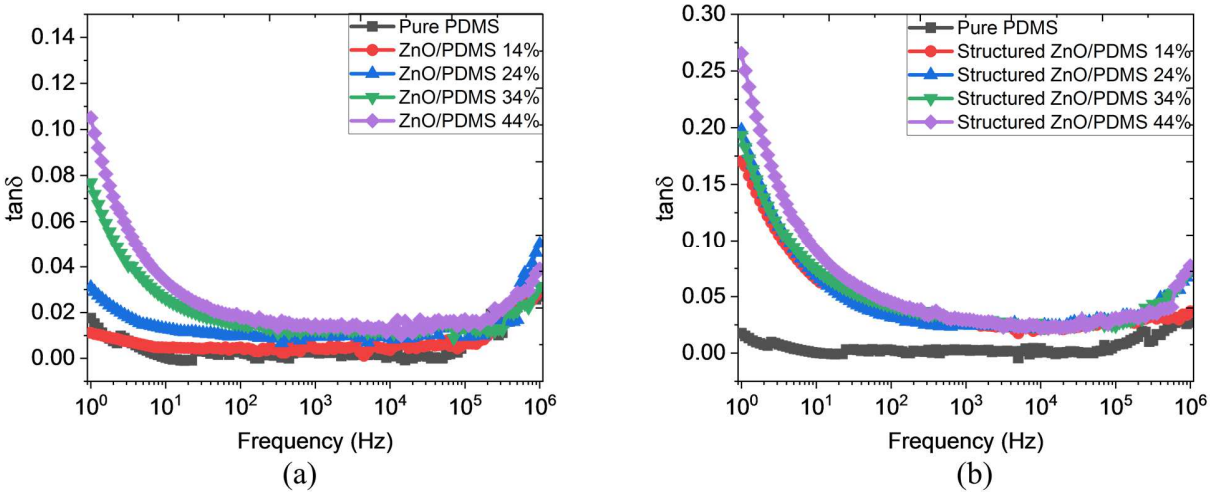

Figure 14. (a) Evolution of dielectric losses of ZnO-PDMS microcomposites with different volume fraction as a function of frequency: (a) without dielectrophoresis process, and (b) with dielectrophoresis process.

The Figure 12e–h-based Comsol simulation highlights the piezoelectric effect, by which the material generates an electric potential in response to an application of mechanical stress in the poling direction. The piezoelectric charge constant d_{33} can be calculated by the so-called coupled equations:

$$S_3 = s_{33}T_3 + d_{33}E_3 \quad (13)$$

$$D_3 = d_{33}T_3 + \varepsilon_{33}E_3 \quad (14)$$

where T_3 is the mechanical compression stress, S_3 is the resulting strain, E_3 and D_3 are, respectively, the electric field strength and the electric displacement, s_{33} is compliance under short-circuit conditions, and ε_{33} is the dielectric constant.

In FEM of Comsol, the ratio of particle size to interparticle distance (r) is one of relevant parameters that strongly affect to the piezoelectric response. Thus, two configurations are performed in this study, including:

- the particles touch themselves ($r = \infty$);
- the particles are spaced equally of 0.05 µm distance ($r = 200$).

As an alternative to the estimation obtained by the Comsol Multiphysics model, the charge coefficient d_{33} can be measured using the experimental setup previously described in Figure 9. A comparison of the d_{33} value between aligned and random PDMS/ZnO composites elaborated with different concentrations is revealed in Figure 15. The result confirms that the dielectrophoretic orientation on ZnO particles successfully enhances the piezoelectric response of the structured composite as opposed to the 0-3 composite. Exceptionally, at a low volume fraction of 14%, significant enhancement has been recorded, leading to an increase in the charge coefficient from 0.5 to 4. At above 20% of ZnO content, the d_{33} value of the oriented sample slowly increases and seems to attain the saturated regime, which is contrary to the random material whose d_{33} significantly improved with high filler concentration. Nonetheless, at a 44% volume fraction, the 1-3 composite still achieved an almost two-fold increase in the charge coefficient (i.e., 5.2) with respect to the 0-3 one (i.e., 2.7).

The saturation effect appearing in the composite with high piezoelectric-particle content can be explained by the fact that such materials already exhibit high connectivity between ZnO/ZnO interfaces, which cannot be much of an increase anymore, even when being treated with dielectrophoresis. On the other hand, the weak connectivity pattern of the 0-3 composite with low piezoelectric concentration can be significantly enhanced after the dielectrophoretic alignment of particles.

Besides the FEM simulation and experimental measurement, analytical approaches have been investigated to predict the charge coefficient d_{33}. The Yamada model [34] is utilized in 0-3 composites to estimate the d_{33} value along the poling direction:

$$d_{33\,random} = \frac{f_p n \alpha \varepsilon_{eff} d_{33\,p}}{(n-1)\varepsilon_{eff} + \varepsilon_p} \quad (15)$$

where n is a shape-dependent parameter, α is the poling ratio of the particles, and $d_{33\,p}$ is the piezoelectric charge constant of the particles.

The Bowen model can be expanded to the Van den Ende model [36] to calculate the charge coefficient d_{33} of 1-3 composite with particle-matrix alternations in the chains. The equation for d_{33} of such a design architecture is given by:

$$d_{33\,structured} = \frac{(1+r)^2 \varepsilon_m f_p d_{33\,p} Y_p}{(\varepsilon_p + r\varepsilon_m)[(1+rf_p)Y_p + f_m Y_m r]} \quad (16)$$

where r is the ratio of the average particle size to the effective inter-particle distance and Y_p and Y_m are, respectively, the elastic moduli of the particles and matrix in the direction of the chain.

The analytical parameters of Yamada, and Van den Ende models, together with those used in the FEM simulation are displayed in Table 4, based on which theoretical estimation faithfully matches the empirical measurement, as illustrated in Figure 15. Indeed, the best fit between the experimental data and the Van den Ende models allows for the determination of the piezoelectric constant d_{33} of the micro-ZnO particles with a value of approximately 1.45 pC/N (Eq. 15). Injecting this value in the Yamada model leads to an estimation of the poling ratio α and the shape-dependent parameter n (Eq. 16). The quality of all theoretical models was verified by the coefficient of determination R^2, which almost equals 1.

Interestingly, Comsol simulation leads to very different values of d_{33p}, i.e. 0.73 pC/N and 2.35 pC/N, corresponding to the ratio r equals ∞ and 200, respectively. These values (d_{33p}) are not the same to the one found from the analytical equations (i.e., 1.45). This is probably because the ideal position of the particles imposed in a 3D Comsol design is far from the their irregular position, even if all particles chains are quite aligned thanks to dielectrophoresis technique. As the inter-particle distance is not easy to be determined in a 3D architecture, we consider in the FEM that all particles within a chain connect together or being spaced from each other by a constant distance. Regarding the theoretical analytic models of Yamada and Van den Ende, on the other hand, only a simple 2D architecture is considered where the inter-particle distance is easier to be estimated. As a result, the average inter-particle distance, which significantly affects to the piezoelectric response, is very different between the 2D analytical model (applied for the macroscopic composite) and the 3D Comsol simulation (applied for the microscopic unit cell).

Table 4. Fitting d_{33}-based various models for structured and random micro-ZnO/PDMS composites

Model	$\boldsymbol{\varepsilon_m}$	$\boldsymbol{\varepsilon_p}$	$\mathbf{d_{33p}}$ (pC/N)	**α**	**n**	**r**	$\boldsymbol{Y_p}$(GPa)	$\boldsymbol{Y_m}$(MPa)	$\boldsymbol{R^2}$
Yamada	2.68	125	1.45	1.01 ± 0.05	6.63	-	-	-	0.978
Van den Ende	2.68	125	1.45 ± 0.02	-	-	24.28	127	0.75	0.995
Comsol	2.68	218	0.73	-	-	∞	127	0.75	0.984
Comsol	2.68	218	2.35	-	-	200	127	0.75	0.998

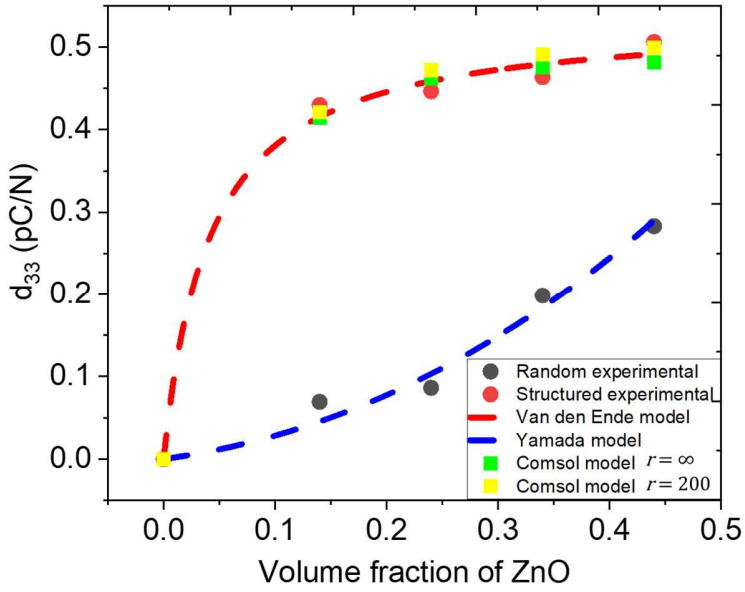

Figure 15. Experimental and fitting piezoelectric coefficients (d_{33}) of structured and random micro-ZnO/PDMS composites as a function of ZnO concentration under 1kHz mechanical excitation. The dotted lines represent the empirically measured values, the square lines correspond to the Comsol simulation, and the dashed lines depict the theoretical models.

6. CONCLUSION

In this work, a dielectrophoretic structuring technique was explored for micro-ZnO/PDMS composite and it was confirmed that this technique can be used to induce directional materials properties. Indeed, the structuration of particles is considered to be one of the key factors governing both dielectric and piezoelectric properties of composites, which were demonstrated to be significantly improved through experimental tests as well as theoretical work. Several analytic models were fitted to the real data and good coherent was observed, reflecting a high reliability of the proposed approaches. A microscopic observation of chain-like particle structure along the field direction was successfully achieved in a non-cured state of composites. Additionally, the effect of processing parameters, such as amplitude and frequency of the applied electric field on alignment of ZnO particles was investigated to determine the best configuration for the dielectrophoretic process. Besides an estimation of the relative permittivity (ε_p) as well as the charge coefficient (d_{33p}) of ZnO particles, another physical parameter (r) relating to effective inter-particle distance was predicted thanks to analytical models. This study also reports on FEM using a Comsol simulation in order to better assess the effect of a 3D architecture device on methods of estimation. Future research should investigate more complex material designs based on ZnO ordered nanowire networks. Such configurations have various advantages over other film-type or bulky materials due to their high specific surface area, well-oriented uniform crystal structures, and directed charge transport paths that enable high device performance and enhanced piezoelectric behavior. SEM characterization will be envisaged to better observe composition and morphology of composite materials. Another aspect of this study consisted of exploring different multiphysic coupling of ZnO materials in order to validate its feasibility for various applications, for instance, flexible sensors adapted to biological media.

Acknowledgements

This work is supported by the ANR (French National Research Agency): ANR-19-CE45-0020-05, ROLLER project, coordinator: Lionel PETIT.

Declaration of competing interest

The authors have no conflicts of interest to declare.

Authors contribution

XZ and MQL wrote and edited the manuscript. XZ performed all experimental test, plotted data, elaborated composites, and developed the Comsol simulation. MQL provided language help and supervised research. PJC developed the experimental setup and provided help analyzing data. OZ provided technical assistance and JFC gave advice on the Comsol simulation. LP validated the feasibility of the project and financed the research.

References

[1] N. Della Schiava, K. Thetpraphi, M.-Q. Le, P. Lermusiaux, A. Millon, J.-F. Capsal, P.-J. Cottinet, Enhanced Figures of Merit for a High-Performing Actuator in Electrostrictive Materials, Polymers. 10 (2018) 263. https://doi.org/10.3390/polym10030263.

[2] Z. Xiang, B. Ducharne, N. Della Schiava, J.-F. Capsal, P.-J. Cottinet, G. Coativy, P. Lermusiaux, M.Q. Le, Induction heating-based low-frequency alternating magnetic field: High potential of ferromagnetic composites for medical applications, Materials & Design. 174 (2019) 107804. https://doi.org/10.1016/j.matdes.2019.107804.

[3] K. Thetpraphi, M.Q. Le, A. Houachtia, P.-J. Cottinet, L. Petit, D. Audigier, J. Kuhn, G. Moretto, J.-F. Capsal, Surface Correction Control Based on Plasticized Multilayer P(VDF-TrFE-CFE) Actuator—Live Mirror, Advanced Optical Materials. 7 (2019) 1900210. https://doi.org/10.1002/adom.201900210.

[4] F. Pedroli, A. Marrani, M.-Q. Le, C. Froidefond, P.-J. Cottinet, J.-F. Capsal, Processing optimization: A way to improve the ionic conductivity and dielectric loss of electroactive polymers, Journal of Polymer Science Part B: Polymer Physics. 56 (2018) 1164–1173. https://doi.org/10.1002/polb.24636.

[5] K. Furusawa, K. Nagashima, C. Anzai, Synthetic process to control the total size and component distribution of multilayer magnetic composite particles, Colloid & Polymer Science. 272 (1994) 1104–1110. https://doi.org/10.1007/BF00652379.

[6] E. Duguet, M. Abboud, F. Morvan, P. Maheu, M. Fontanille, PMMA encapsulation of alumina particles through aqueous suspension polymerisation processes, Macromolecular Symposia. 151 (2000) 365–370. https://doi.org/10.1002/1521-3900(200002)151:1<365::AID-MASY365>3.0.CO;2-T.

[7] S. Hayashi, K. Fujiki, N. Tsubokawa, Grafting of hyperbranched polymers onto ultrafine silica: Postgraft polymerization of vinyl monomers initiated by pendant initiating groups of polymer chains grafted onto the surface, Reactive and Functional Polymers. 46 (2000) 193–201. https://doi.org/10.1016/S1381-5148(00)00053-5.

[8] Z. Xiang, K.-I. Jakkpat, B. Ducharne, J.-F. Capsal, J.-F. Mogniotte, P. Lermusiaux, P.-J. Cottinet, N. Della Schiava, M.Q. Le, Enhancing the Low-Frequency Induction Heating Effect of Magnetic Composites for Medical Applications, Polymers. 12 (2020) 386. https://doi.org/10.3390/polym12020386.

[9] M. Mokni, F. Pedroli, G. D'Ambrogio, M.-Q. Le, P.-J. Cottinet, J.-F. Capsal, High-Capacity, Fast-Response, and Photocapacitor-Based Terpolymer Phosphor Composite, Polymers. 12 (2020) 349. https://doi.org/10.3390/polym12020349.

[10] K. Thetpraphi, M.Q. Le, A. Houachtia, P.J. Cottinet, L. Petit, D. Audigier, J. Kuhn, G. Moretto, J.F. Capsal, Surface Correction Control Based on Plasticized Multilayer P(VDF-TrFE-CFE) Actuator—Live Mirror, Advanced Optical Materials. 7 (2019) 1900210. https://doi.org/10.1002/adom.201900210.

[11] Q. Liu, M.Q. Le, C. Richard, R. Liang, P.J. Cottinet, J.F. Capsal, Enhanced pseudo-piezoelectric dynamic force sensors based on inkjet-printed electrostrictive terpolymer, Organic Electronics. 67 (2019) 259–271. https://doi.org/10.1016/j.orgel.2019.01.028.

[12] D. Grinberg, S. Siddique, M.Q. Le, R. Liang, J.F. Capsal, P.J. Cottinet, 4D Printing based piezoelectric composite for medical applications, Journal of Polymer Science, Part B: Polymer Physics. 57 (2019) 109–115. https://doi.org/10.1002/polb.24763.

[13] M.Q. Le, F. Belhora, A. Cornogolub, P.J. Cottinet, L. Lebrun, A. Hajjaji, Enhanced magnetoelectric effect for flexible current sensor applications, Journal of Applied Physics. 115 (2014) 194103. https://doi.org/10.1063/1.4876910.

[14] M.Q. Le, J.F. Capsal, J. Galineau, F. Ganet, X. Yin, M.D. Yang, J.F. Chateaux, L. Renaud, C. Malhaire, P.J. Cottinet, R. Liang, All-organic electrostrictive polymer composites with low driving electrical voltages for micro-fluidic pump applications, Scientific Reports. 5 (2015) 1–13. https://doi.org/10.1038/srep11814.

[15] F. Ganet, M.Q. Le, J.F. Capsal, J.F. Gérard, S. Pruvost, J. Duchet-Rumeau, S. Livi, P. Lermusiaux, A. Millon, P.J. Cottinet, Haptic feedback using an all-organic electroactive polymer composite, Sensors and Actuators, B: Chemical. 220 (2015) 1120–1130. https://doi.org/10.1016/j.snb.2015.06.071.

[16] J. DeGraff, R. Liang, M.Q. Le, J.-F. Capsal, F. Ganet, P.-J. Cottinet, Printable low-cost and flexible carbon nanotube buckypaper motion sensors, Materials & Design. 133 (2017) 47–53. https://doi.org/10.1016/j.matdes.2017.07.048.

[17] D. Grinberg, S. Siddique, M.-Q. Le, R. Liang, J.-F. Capsal, P.-J. Cottinet, 4D Printing based piezoelectric composite for medical applications, Journal of Polymer Science Part B: Polymer Physics. 57 (2019) 109–115. https://doi.org/10.1002/polb.24763.

[18] F. Momeni, S. M.Mehdi Hassani.N, X. Liu, J. Ni, A review of 4D printing, Materials & Design. 122 (2017) 42–79. https://doi.org/10.1016/j.matdes.2017.02.068.

[19] K. Thetpraphi, G. Moretto, J.R. Kuhn, P.J. Cottinet, M.Q. Le, D. Audigier, L. Petit, J.F. Capsal, Advanced 3D-printed EAP actuator applied to high precision large optical-quality surface fabrication: first results, in: Electroactive Polymer Actuators and Devices (EAPAD) XXII, International Society for Optics and Photonics, 2020: p. 113751X. https://doi.org/10.1117/12.2556532.

[20] Q. Liu, M.Q. Le, C. Richard, R. Liang, P.-J. Cottinet, J.-F. Capsal, Enhanced pseudo-piezoelectric dynamic force sensors based on inkjet-printed electrostrictive terpolymer, Organic Electronics. 67 (2019) 259–271. https://doi.org/10.1016/j.orgel.2019.01.028.

[21] M.S. Arnold, P. Avouris, Z.W. Pan, Z.L. Wang, Field-effect transistors based on single semiconducting oxide nanobelts, Journal of Physical Chemistry B. 107 (2003) 659–663. https://doi.org/10.1021/jp0271054.

[22] M.H. Huang, S. Mao, H. Feick, H. Yan, Y. Wu, H. Kind, E. Weber, R. Russo, P. Yang, Room-temperature ultraviolet nanowire nanolasers, Science. 292 (2001) 1897–1899. https://doi.org/10.1126/science.1060367.

[23] † C. Soci, † A. Zhang, B. Xiang, S. A. Dayeh, D. P. R. Aplin, J. Park, X. Y. Bao, and Y. H. Lo, D. Wang*, ZnO Nanowire UV Photodetectors with High Internal Gain, (2007). https://doi.org/10.1021/NL070111X.

[24] W.I. Park, G.-C. Yi, Electroluminescence in n-ZnO Nanorod Arrays Vertically Grown on p-GaN, Advanced Materials. 16 (2004) 87–90. https://doi.org/10.1002/adma.200305729.

[25] M. Law, L.E. Greene, J.C. Johnson, R. Saykally, P. Yang, Nanowire dye-sensitized solar cells, Nature Materials. 4 (2005) 455–459. https://doi.org/10.1038/nmat1387.

[26] B.A. Buchine, W.L. Hughes, F.L. Degertekin, Z.L. Wang, Bulk acoustic resonator based on piezoelectric ZnO belts, Nano Letters. 6 (2006) 1155–1159. https://doi.org/10.1021/nl060351x.

[27] S.C. Tjong, G.D. Liang, Electrical properties of low-density polyethylene/ZnO nanocomposites, Materials Chemistry and Physics. 100 (2006) 1–5. https://doi.org/10.1016/j.matchemphys.2005.11.029.

[28] A. Matei, I. Cernica, O. Cadar, C. Roman, V. Schiopu, Synthesis and characterization of ZnO - polymer nanocomposites, International Journal of Material Forming. 1 (2008) 767–770. https://doi.org/10.1007/s12289-008-0288-5.

[29] E. Tang, G. Cheng, X. Pang, X. Ma, F. Xing, Synthesis of nano-ZnO/poly(methyl methacrylate) composite microsphere through emulsion polymerization and its UV-shielding property, Colloid and Polymer Science. 284 (2006) 422–428. https://doi.org/10.1007/s00396-005-1389-z.

[30] K.J. Loh, D. Chang, Zinc oxide nanoparticle-polymeric thin films for dynamic strain sensing, Journal of Materials Science. 46 (2011) 228–237. https://doi.org/10.1007/s10853-010-4940-3.

[31] S. Jiansirisomboon, K. Songsiri, A. Watcharapasorn, T. Tunkasiri, Mechanical properties and crack growth behavior in poled ferroelectric PMN-PZT ceramics, Current Applied Physics. 6 (2006) 299–302. https://doi.org/10.1016/j.cap.2005.11.004.

[32] T.T. Wang, J.M. Herbert, A.M. (Alastair M.) Glass, The Applications of ferroelectric polymers, Blackie, 1988.

[33] R.E. Newnham, D.P. Skinner, L.E. Cross, Connectivity and piezoelectric-pyroelectric composites, Materials Research Bulletin. 13 (1978) 525–536. https://doi.org/10.1016/0025-5408(78)90161-7.

[34] T. Yamada, T. Ueda, T. Kitayama, Piezoelectricity of a high-content lead zirconate titanate/polymer composite, Journal of Applied Physics. 53 (1982) 4328–4332. https://doi.org/10.1063/1.331211.

[35] A. Safari, Development of piezoelectric composites for transducers, Journal de Physique. III. 4 (1994) 1129–1149. https://doi.org/10.1051/jp3:1994191.

[36] D.A. Van Den Ende, B.F. Bory, W.A. Groen, S. Van Der Zwaag, Improving the d33 and g33 properties of 0-3 piezoelectric composites by dielectrophoresis, Journal of Applied Physics. 107 (2010) 0–8. https://doi.org/10.1063/1.3291131.

[37] D.Y. Wang, K. Li, H.L.W. Chan, High frequency 1-3 composite transducer fabricated using sol-gel derived lead-free BNBT fibers, Sensors and Actuators, A: Physical. 114 (2004) 1–6. https://doi.org/10.1016/j.sna.2004.02.024.

[38] A. Abrar, D. Zhang, B. Su, T.W. Button, K.J. Kirk, S. Cochran, 1-3 Connectivity piezoelectric ceramic-polymer composite transducers made with viscous polymer processing for high frequency ultrasound, in: Ultrasonics, 2004: pp. 479–484. https://doi.org/10.1016/j.ultras.2004.02.008.

[39] C.P. Bowen, R.E. Newnham, C.A. Randall, Dielectric properties of dielectrophoretically assembled particulate-polymer composites, Journal of Materials Research. 13 (1998) 205–210. https://doi.org/10.1557/JMR.1998.0027.

[40] N.K. James, D.B. Deutz, R.K. Bose, S. van der Zwaag, P. Groen, High Piezoelectric Voltage Coefficient in Structured Lead-Free (K,Na,Li)NbO_3 Particulate-Epoxy Composites, Journal of the American Ceramic Society. 99 (2016) 3957–3963. https://doi.org/10.1111/jace.14428.

[41] A. Al Masud, N. D'Souza, P. Von Lockette, Z. Ounaies, On the dielectrophoretic and magnetic alignment of magnetoactive barium hexaferrite-pdms nanocomposites, ASME 2017 Conference on Smart Materials, Adaptive Structures and Intelligent Systems, SMASIS 2017. 1 (2017). https://doi.org/10.1115/SMASIS2017-3988.

[42] C. Park, Z. Ounaies, K.A. Watson, R.E. Crooks, J. Smith, S.E. Lowther, J.W. Connell, E.J. Siochi, J.S. Harrison, T.L. St Clair, Dispersion of single wall carbon nanotubes by in situ polymerization under sonication, Chemical Physics Letters. 364 (2002) 303–308. https://doi.org/10.1016/S0009-2614(02)01326-X.

[43] L. An, C.R. Friedrich, Process parameters and their relations for the dielectrophoretic assembly of carbon nanotubes, Journal of Applied Physics. 105 (2009). https://doi.org/10.1063/1.3093975.

[44] D.A. Van Den Ende, S.E. Van Kempen, X. Wu, W.A. Groen, C.A. Randall, S. Van Der Zwaag, Dielectrophoretically structured piezoelectric composites with high aspect ratio piezoelectric particles inclusions, Journal of Applied Physics. 111 (2012). https://doi.org/10.1063/1.4729814.

[45] H. Khanbareh, S. Van Der Zwaag, W.A. Groen, Effect of dielectrophoretic structuring on piezoelectric and pyroelectric properties of lead titanate-epoxy composites, Smart Materials and Structures. 23 (2014). https://doi.org/10.1088/0964-1726/23/10/105030.

[46] D.A. Van Den Ende, B.F. Bory, W.A. Groen, S. Van Der Zwaag, Properties of quasi 1-3 piezoelectric PZT-epoxy composites obtained by dielectrophoresis, in: Integrated Ferroelectrics, 2010: pp. 108–118. https://doi.org/10.1080/10584587.2010.488525.

[47] C.A. Randall, S. Miyazaki, K.L. More, A.S. Bhalla, R.E. Newnham, Structural-property relationships in dielectrophoretically assembled BaTiO3 nanocomposites, Materials Letters. 15 (1992) 26–30. https://doi.org/10.1016/0167-577X(92)90006-6.

[48] G. Belijar, S. Diaham, Z. Valdez-Nava, T. Lebey, Online optical and dielectric monitoring of anisotropic epoxy/BaTiO3composite formation tailored by dielectrophoresis, J. Phys. D: Appl. Phys. 49 (2015) 045501. https://doi.org/10.1088/0022-3727/49/4/045501.

[49] Sybrandvan der Zwaag, Dan A. van den Ende, Wilhelm Albert (Pim) Groen, Sensing and Energy Harvesting Novel Polymer Composites, Materials Experience. (2014) 221–234. https://doi.org/10.1016/B978-0-08-099359-1.00016-3.

[50] G.O.F. Parikesit, A.P. Markesteijn, O.M. Piciu, A. Bossche, J. Westerweel, I.T. Young, Y. Garini, Size-dependent trajectories of DNA macromolecules due to insulative dielectrophoresis in submicrometer-deep fluidic channels, Biomicrofluidics. 2 (2008) 024103. https://doi.org/10.1063/1.2930817.

[51] S. Ozuna-Chacón, B.H. Lapizco-Encinas, M. Rito-Palomares, S.O. Martínez-Chapa, C. Reyes-Betanzo, Performance characterization of an insulator-based dielectrophoretic microdevice, Electrophoresis. 29 (2008) 3115–3122. https://doi.org/10.1002/elps.200700865.

[52] J. Kim, Y.-H. Shin, J.-H. Yun, C.-S. Han, M.S. Hyun, W.A. Anderson, A nickel silicide nanowire microscopy tip obtains nanoscale information, Nanotechnology. 19 (2008) 485713. https://doi.org/10.1088/0957-4484/19/48/485713.

[53] L. Zheng, J.P. Brody, P.J. Burke, Electronic manipulation of DNA, proteins, and nanoparticles for potential circuit assembly, Biosensors and Bioelectronics. 20 (2004) 606–619.

[54] M. Yang, X. Zhang, Electrical assisted patterning of cardiac myocytes with controlled macroscopic anisotropy using a microfluidic dielectrophoresis chip, Sensors and Actuators A: Physical. 135 (2007) 73–79.

[55] D.R. Albrecht, V.L. Tsang, R.L. Sah, S.N. Bhatia, Photo- and electropatterning of hydrogel-encapsulated living cell arrays, Lab Chip. 5 (2005) 111–118. https://doi.org/10.1039/b406953f.

[56] X. Liu, J.L. Spencer, A.B. Kaiser, W.M. Arnold, Selective purification of multiwalled carbon nanotubes by dielectrophoresis within a large array, Current Applied Physics. 6 (2006) 427–431.

[57] H. Li, Y. Zheng, D. Akin, R. Bashir, Characterization and modeling of a microfluidic dielectrophoresis filter for biological species, Journal of Microelectromechanical Systems. 14 (2005) 103–112.

[58] S. Basuray, H.-C. Chang, Induced dipoles and dielectrophoresis of nanocolloids in electrolytes, Physical Review E. 75 (2007) 060501.

[59] P.R.C. Gascoyne, J. Vykoukal, Particle separation by dielectrophoresis, ELECTROPHORESIS. 23 (2002) 1973–1983. https://doi.org/10.1002/1522-2683(200207)23:13<1973::AID-ELPS1973>3.0.CO;2-1.

[60] M.L. Terranova, M. Lucci, S. Orlanducci, E. Tamburri, V. Sessa, A. Reale, A. Di Carlo, Carbon nanotubes for gas detection: materials preparation and device assembly, Journal of Physics: Condensed Matter. 19 (2007) 225004.

[61] J.-W. Lee, K.-J. Moon, M.-H. Ham, J.-M. Myoung, Dielectrophoretic assembly of GaN nanowires for UV sensor applications, Solid State Communications. 148 (2008) 194–198.

[62] V. La Ferrara, B. Alfano, E. Massera, G. Di Francia, Palladium nanowires assembly by dielectrophoresis investigated as hydrogen sensors, IEEE Transactions on Nanotechnology. 7 (2008) 776–781.

[63] N. Chimot, V. Derycke, M.F. Goffman, J.P. Bourgoin, H. Happy, G. Dambrine, Gigahertz frequency flexible carbon nanotube transistors, Applied Physics Letters. 91 (2007) 153111.

[64] S.C. Wang, H. Yang, S. Banerjee, I.P. Herman, D.L. Akins, AOT dispersed single-walled carbon nanotubes for transistor device application, Materials Letters. 62 (2008) 843–845.

[65] A.A. Pesetski, J.E. Baumgardner, S.V. Krishnaswamy, H. Zhang, J.D. Adam, C. Kocabas, T. Banks, J.A. Rogers, A 500 MHz carbon nanotube transistor oscillator, Applied Physics Letters. 93 (2008) 123506.

[66] C.S. Lao, J. Liu, P. Gao, L. Zhang, D. Davidovic, R. Tummala, Z.L. Wang, ZnO nanobelt/nanowire Schottky diodes formed by dielectrophoresis alignment across Au electrodes, Nano Letters. 6 (2006) 263–266.

[67] S.-Y. Lee, T.-H. Kim, D.-I. Suh, E.-K. Suh, N.-K. Cho, W.-K. Seong, S.-K. Lee, Dielectrophoretically aligned GaN nanowire rectifiers, Applied Physics A. 87 (2007) 739–742.

[68] C. Zhang, K. Khoshmanesh, A. Mitchell, K. Kalantar-Zadeh, Dielectrophoresis for manipulation of micro/nano particles in microfluidic systems, Anal Bioanal Chem. 396 (2010) 401–420. https://doi.org/10.1007/s00216-009-2922-6.

[69] M.A. Al Masud, Z. Ounaies, Dielectric properties of dielectrophoretically aligned ZNO-PDMS composites, in: ASME 2016 Conference on Smart Materials, Adaptive Structures and Intelligent Systems, SMASIS 2016, American Society of Mechanical Engineers, 2016. https://doi.org/10.1115/SMASIS2016-9128.

[70] S. Kumar, Y.K. Seo, G.H. Kim, Manipulation and trapping of semiconducting ZnO nanoparticles into nanogap electrodes by dielectrophoresis technique, Applied Physics Letters. 94 (2009) 153104. https://doi.org/10.1063/1.3118588.

[71] A.S. Dukhin, Z.R. Ulberg, T.G. Gruzina, V.I. Karamushka, Peculiarities of live cells' interaction with micro- and nanoparticles, in: Colloid and Interface Science in Pharmaceutical Research and Development, Elsevier Inc., 2014: pp. 193–222. https://doi.org/10.1016/B978-0-444-62614-1.00010-7.

[72] T.B. Jones, Electromechanics of Particles, Cambridge University Press, 1995. https://doi.org/10.1017/cbo9780511574498.

[73] F. Pedroli, A. Flocchini, A. Marrani, M.-Q. Le, O. Sanseau, P.-J. Cottinet, J.-F. Capsal, Boosted energy-storage efficiency by controlling conduction loss of multilayered polymeric capacitors, Materials & Design. 192 (2020) 108712. https://doi.org/10.1016/j.matdes.2020.108712.

[74] C. Liu, A.J. Bard, Pressure-induced insulator conductor transition in a photoconducting organic liquid-crystal film, Nature. 418 (2002) 162–164. https://doi.org/10.1038/nature00875.

[75] H. Ahmad, A. Haddad, H. Griffiths, S. Robson, T. Nishimura, N. Tsukamoto, Electrical characterisation of ZnO microvaristor materials and compounds, in: 2015 IEEE Conference on Electrical Insulation and Dielectric Phenomena (CEIDP), 2015: pp. 688–692. https://doi.org/10.1109/CEIDP.2015.7352035.

[76] G.C. Psarras, Fundamentals of Dielectric Theories, in: Dielectric Polymer Materials for High-Density Energy Storage, Elsevier, 2018: pp. 11–57. https://doi.org/10.1016/b978-0-12-813215-9.00002-6.

[77] J.F. Capsal, J. Galineau, M.Q. Le, F. Domingues Dos Santos, P.J. Cottinet, Enhanced electrostriction based on plasticized relaxor ferroelectric P(VDF-TrFE-CFE/CTFE) blends, Journal of Polymer Science, Part B: Polymer Physics. 53 (2015) 1368–1379. https://doi.org/10.1002/polb.23776.

[78] J.I. Hong, P. Winberg, L.S. Schadler, R.W. Siegel, Dielectric properties of zinc oxide/low density polyethylene nanocomposites, Materials Letters. 59 (2005) 473–476. https://doi.org/10.1016/j.matlet.2004.10.036.

[79] J.C.M. Garnett, Colours in Metal Glasses and in Metallic Films, Philosophical Transactions of the Royal Society A: Mathematical, Physical and Engineering Sciences. 203 (1904) 385–420. https://doi.org/10.1098/rsta.1904.0024.

[80] K. Mazur, Polymer-ferroelectric ceramic composites, PLASTICS ENGINEERING-NEW YORK. 28 (1995) 539.

[81] N. Jayasundere, B. V. Smith, Dielectric constant for binary piezoelectric 0-3 composites, Journal of Applied Physics. 73 (1993) 2462–2466. https://doi.org/10.1063/1.354057.

[82] S. Liu, S. Xiu, B. Shen, J. Zhai, L.B. Kong, Dielectric properties and energy storage densities of poly(vinylidenefluoride) nanocomposite with surface hydroxylated cube shaped Ba0.6Sr0.4TiO3 nanoparticles, Polymers. 8 (2016) 10–14. https://doi.org/10.3390/polym8020045.

[83] T.S. Velayutham, W.H. Abd Majid, W.C. Gan, A. Khorsand Zak, S.N. Gan, Theoretical and experimental approach on dielectric properties of ZnO nanoparticles and polyurethane/ZnO nanocomposites, Journal of Applied Physics. 112 (2012). https://doi.org/10.1063/1.4749414.

[84] A. Sihvola, Mixing Rules with Complex Dielectric Coefficients, Subsurface Sensing Technologies and Applications. 1 (2000) 393–415. https://doi.org/10.1023/A:1026511515005.

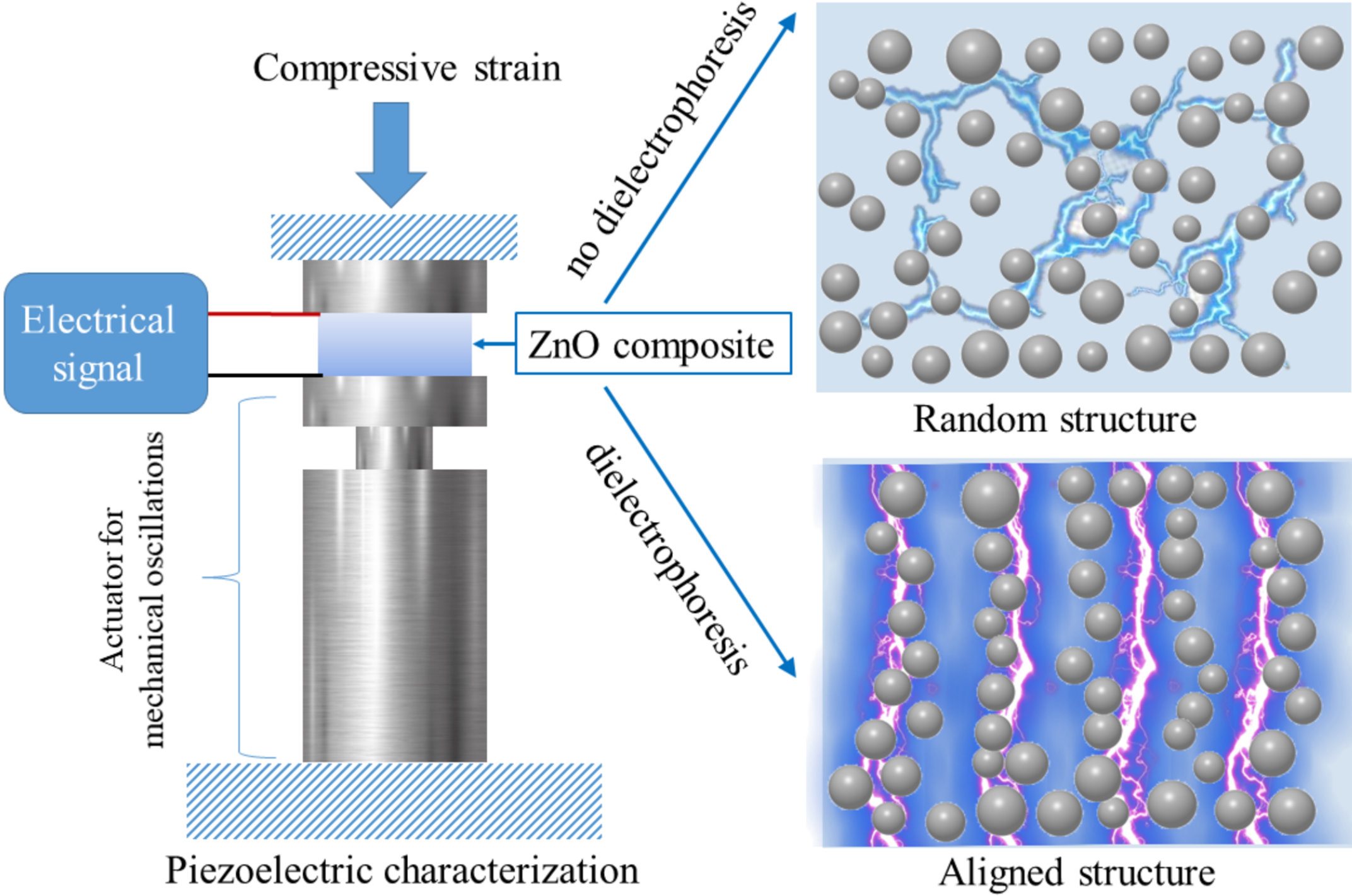
Compressive strain
Electrical signal
ZnO composite
Actuator for mechanical oscillations
Piezoelectric characterization
no dielectrophoresis
dielectrophoresis
Random structure
Aligned structure